BASE TRANSIT TIME OF A Si/SiGe HBT CONSIDERING GAUSSIAN DOPED BASE

S. M. MOUDUDUL ISLAM

DEPARTMENT OF ELECTRICAL & ELECTRONIC ENGINEERING

BUET, DHAKA
2010

Base Transit Time of a Si/SiGe HBT Considering Gaussian Doped Base

By
S. M. Moududul Islam

A thesis submitted to the Department of Electrical and Electronic Engineering
Bangladesh University of Engineering & Technology
in partial fulfillment of the requirements
for the degree of

MASTER OF SCIENCE IN ELECTRICAL AND ELECTRONIC ENGINEERING

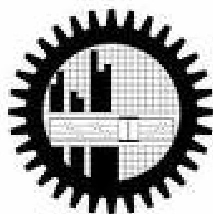

DEPARTMENT OF ELECTRICAL & ELECTRONIC ENGINEERING
BANGLADESH UNIVERSITY OF ENGINEERING AND TECHONOLGY, DHAKA
2010

CERTIFICATION

The thesis titled **"BASE TRANSIT TIME OF A Si/SiGe HBT CONSIDERING GAUSSIAN DOPED BASE"** submitted by S. M. Moududul Islam, Roll No.: 100706204P, Session: October, 2007 has been accepted as satisfactory in partial fulfillment of the requirements for the degree of MASTER OF SCIENCE IN ELECTRICAL AND ELECTRONIC ENGINEERING on August 04, 2010.

BOARD OF EXAMINERS

1. ____
(Dr. Md. Ziaur Rahman Khan) — **Chairman** (Supervisor)
Associate Professor,
Department of Electrical and Electronic Engineering,
Bangladesh University of Engineering & Technology,
Dhaka-1000, Bangladesh.

2. ____
(Dr. Md. Saifur Rahman) — **Member** (Ex-Officio)
Professor and Head,
Department of Electrical and Electronic Engineering,
Bangladesh University of Engineering & Technology,
Dhaka-1000, Bangladesh.

3. ____
(Dr. Sharif Mohammad Mominuzzaman) — **Member**
Professor,
Department of Electrical and Electronic Engineering,
Bangladesh University of Engineering & Technology,
Dhaka-1000, Bangladesh.

4. ____
(Dr. Md. Anwarul Abedin) — **Member** (External)
Associate Professor,
Department of Electrical and Electronic Engineering,
Dhaka University of Engineering & Technology,
Gazipur, Bangladesh.

DECLARATION

It is hereby declared that this thesis or any part of it has not been submitted elsewhere for the award of any degree or diploma.

Signature of the candidate

____

(S. M. Moududul Islam)

<u>DEDICATION</u>

To my beloved parents…

TABLE OF CONTENTS

			Page No.
TITLE PAGE			i
CERTIFICATION			ii
DECLARATION			iii
DEDICATION			iv
LIST OF FIGURES			viii
ACKNOWLEDGMENTS			x
ABSTRACT			xi
CHAPTER	**1**	**INTRODUCTION**	**1**
	1.1	TRANSISTOR	1
	1.1.1	History in brief	1
	1.2	REVIEW OF RECENT WORK	3
	1.3	SCOPE OF THIS DISSERTATION	6
	1.4	CHAPTER LAYOUT	7
CHAPTER	**2**	**BACKGROUND**	**8**
	2.1	TRANSISTOR CATEGORIES	8
	2.2	BIPOLAR TRANSISTOR	9
	2.2.1	Dopants	9
	2.2.2	Doping process	10
	2.2.3	The n^+-p-n transistor	10
	2.2.4	Suitability of bipolar transistor	11
	2.3	HETEROJUNCTION BIPOLAR TRANSISTOR	12
	2.3.1	SiGe device physics	13
	2.3.2	SiGe HBT	17
	2.3.3	Comparison between RFIC technologies	19
	2.4	BASE TRANSIT TIME	21
CHAPTER	**3**	**MATHEMATICAL ANALYSIS**	**23**
	3.1	INTRODUCTION	23

	3.2	DERIVATION OF MODEL EQUATIONS	24
	3.2.1	Low injection model	29
	3.2.2	Model for moderate level of injection	31
	3.3	CONCLUSION	34
CHAPTER	**4**	**RESULTS AND DISCUSSION**	**35**
	4.1	INTRODUCTION	35
	4.2	RESULTS AND DISCUSSION	35
	4.2.1	Distribution of minority carrier within the base	35
	4.2.2	Variation of minority carrier injection ratio with base-emitter voltage	37
	4.2.3	Variation of collector current density with base-emitter voltage	40
	4.2.4	Variation of base transit time with base-emitter voltage	41
	4.2.5	Variation of base transit time with minority carrier injection ratio	42
	4.2.6	Dependence of base transit time upon base width	43
	4.2.7	Dependence of base transit time upon peak base doping concentration	45
	4.2.8	Dependence of base transit time upon field dependent mobility	45
	4.2.9	Dependence of base transit time upon slope of base doping	46
	4.2.10	Dependence of base transit time upon peak Ge fraction	47
	4.2.11	Dependence of base transit time upon collector current Density	48
	4.2.12	Comparison of base transit time with HBT	49
	4.2.13	Comparison of collector current with BJT	49
	4.2.14	Comparison of transit time and current density with BJT	50
	4.3	CONCLUSION	53

CHAPTER	**5**	**CONCLUSION AND SUGGESTIONS**	**54**
	5.1	CONCLUSION	54
	5.2	SUGGESTIONS FOR FUTURE WORK	54
REFERENCES			**56**
APPENDIX	**A**	**DERIVATION FOR LOW INJECTION**	**61**
APPENDIX	**B**	**DERIVATION FOR MODERATE INJECTION**	**66**

LIST OF FIGURES

Name	Caption	Page No.
Figure 1.1	(a) A replica of the first working transistor (b) Transistor and Integrated Circuits (ICs) chronology [Source: Bell Labs].	2
Figure 2.2	The schematic diagram of an n^{+}-p-n bipolar junction transistor. Conventional direction of current flow is assumed.	11
Figure 2.3	The three types of semiconductor heterojunctions organized by band alignment. Here CB stands for conduction band and VB is the valence band.	14
Figure 2.4	Energy band diagram for a graded base SiGe HBT and a Si BJT, biased in forward active mode at low-injection.	14
Figure 1.5	Representative Gummel characteristics for a typical SiGe HBT and a similarly constructed Si BJT	15
Figure 2.6	The schematic diagram showing the cross section of a SiGe heterojunction bipolar transistor.	17
Figure 2.7	Representative base profiles for a first generation SiGe heterojunction bipolar transistor.	19
Figure 3.1	Ge mole fraction distribution within the base of a $Si_{1-y}Ge_y$ HBT for various geometric profiles.	24
Figure 3.2	One-dimensional view of an *npn* SiGe heterojunction bipolar transistor showing flow of injected minority carrier and current density.	25
Figure 3.3	Comparison of injected minority carrier profiles within the base of a $Si_{1-y}Ge_y$ HBT modified from the low injection model ($n_m(x)$) and obtained from numerical solution under moderate injection ($n(x)$). Doping and field dependent mobility is considered.	32
Figure 4.1	Injected electron distribution within the base for different Ge profiles (a) under low injection (V_{be}=0.7V) (b) under moderate injection (V_{be}=0.85V).	36
Figure 4.2	Normalized minority carrier electron distribution within the base (a) for different V_{be} (b) for different $N_B(0)$.	38
Figure 4.3	Normalized minority carrier distribution within the base (a) for different base widths (b) for different slopes of base doping.	39

Name	Caption	Page No.
Figure 4.4	Minority carrier injection ratio as a function of base emitter voltage	40
Figure 4.5	Collector current densities for different shape of Ge profiles as a function of base-emitter voltage.	41
Figure 4.6	Base transit time as a function of base-emitter voltage for different shape of Ge profiles.	42
Figure 4.7	Base transit time as a function of minority carrier injection ratio for box shape Ge profile. Doping dependent mobility is considered.	43
Figure 4.8	Base transit time as function of base width (a) for heavily doped base (b) for a comparatively lightly doped base HBT.	44
Figure 4.9	Base transit time as a function of peak base doping concentration with a box shape Ge profile for moderate and low level of injection.	45
Figure 4.10	Base transit time as a function of base-emitter voltage with and without field dependent electron mobility. A triangular Ge profile is considered.	46
Figure 4.11	Base transit time as a function of slope of base doping with a triangular shape Ge profile for moderate and low level of injection.	47
Figure 4.12	Base transit time as a function of peak Ge % (y_C) for triangular Ge profile with uniform and Gaussian doped base.	48
Figure 4.13	Base transit time as a function of collector current density for different shape of Ge profiles.	49
Figure 4.14	Comparison of base transit time with Ge concentration at the collector edge [26].	50
Figure 4.15	Collector current as a function of base-emitter voltage and b) Difference in collector current as a function of base-emitter voltage for Si BJT and SiGe HBT. The calculated values are compared with Gummel Characteristics reproduced from [34].	51
Figure 4.16	a) Collector current density as a function of base-emitter voltage and b) Base transit time as a function of minority carrier injection ratio for Si BJT. The calculated values are compared with P. Ma results [73].	52

ACKNOWLEDGEMENTS

First of all, I would like to thank Almighty Allah for giving me the opportunity to complete my research work.

I thank my supervisor, Dr. Md. Ziaur Rahman Khan sir, Associate Professor, EEE, BUET. His continuous motivation and all through help in each and every step of my M.Sc. thesis was just phenomenal. I deeply acknowledge his help and contribution till now in fulfilling all the requirements for this thesis.

My heartiest gratitude goes to Yeasir Arafat sir, Assistant Professor, EEE, BUET, for his kind time and suggestions all through the derivations, result analysis etc. I would like to thank him for sharing his thesis which created the pathway for me to go on and produce the results. Basically all my work is based on the formulation of Yeasir Arafat sir, therefore, it's my utmost pleasure in acknowledging him.

I would also like to mention Dr. M. M. Shahidul Hassan sir, as all our work with base transit time for BJT/HBT was initiated by him. In this regard, I would mention Mr. Md. Waliullah Khan Nomani and Mr. Touhidur Rahman, whose earlier work on BJT helped a lot in development of this model.

Mr. Iqbal Bahar Chowdhury, Assistant Professor, United International University, needs special mention for his kind suggestions and time for scrutinizing the detailed derivation steps.

And last but not least, I would like to mention my friend Mr. Md. Nazmul Alam who continuously kept on motivating me with my M.Sc. research and which was really a huge boost in completion of this task.

ABSTRACT

Base transit time of an HBT is more than 70% of its total transit time. Therefore it plays a very crucial role in determining the transistor's high frequency performance. In the present work, base transit time of a Gaussian doped base $Si_{1-y}Ge_y$ HBT with different type of Ge profiles (triangular, trapezoidal and box shape) for low and moderate levels of injection is studied. First of all, a model is developed for low injection only and then using perturbation theory, it is extended to cover moderate level of injection. In doing so, electric field and doping dependent mobility, bandgap narrowing effect due to heavy doping, presence of Ge and change in the density of states, velocity saturation at collector-base junction etc. are considered to study the injected minority carrier, collector current density and stored base charge. Base transit time is calculated numerically using MATLAB as the integrations are quite cumbersome to follow analytical derivations. The results show that base transit time increases with base-emitter voltage, minority carrier injection ratio, base width, peak base doping concentration and if velocity saturation and field dependent mobility is considered. On the other hand base transit time decreases with slope of base doping and gradient in Ge profiles. The results are compared with some available data from literature and published results.

CHAPTER 1

INTRODUCTION AND REVIEW OF LITERATURE

1.1 TRANSISTOR

It is one of the greatest achievements in the 20th century and some consider it one of the most important technological breakthroughs in human history. The transistor is the fundamental building block of modern electronic devices and is used in radio, television, telephone, computer and other electronic systems [1]. Transistor is a semiconductor device commonly used to amplify or switch electronic signals. It is made of a solid piece of a semiconductor material, with multiple terminals for connection to an external circuit. A voltage or current applied to one pair of the transistor's terminals changes the current flowing through another pair of terminals.

1.1.1 History in brief

The first patent for the field-effect transistor principle was filed in Canada by Austrian-Hungarian physicist Julius Edgar Lilienfeld on 22 October 1925 but Lilienfeld did not publish any research articles about his devices [2]. In 1934 German physicist Dr. Oskar Heil patented another field-effect transistor. On 17 November 1947, John Bardeen and Walter Brattain at AT&T Bell Labs observed that when electrical contacts were applied to a crystal of germanium, the output power was larger than the input. William Shockley saw the potential in this invention and as part of a post-war effort to replace vacuum tubes with solid-state devices, worked over the next few months and by December 1947 he greatly succeeded expanding the knowledge of semiconductors. The term “transistor” was coined by John R. Pierce tailoring the words ‘transfer’ & ‘resistor’. According to physicist/historian Robert Arns, legal papers from the Bell Labs patent show that William Shockley and Gerald Pearson had built operational versions from Lilienfeld's patents, yet

(a)

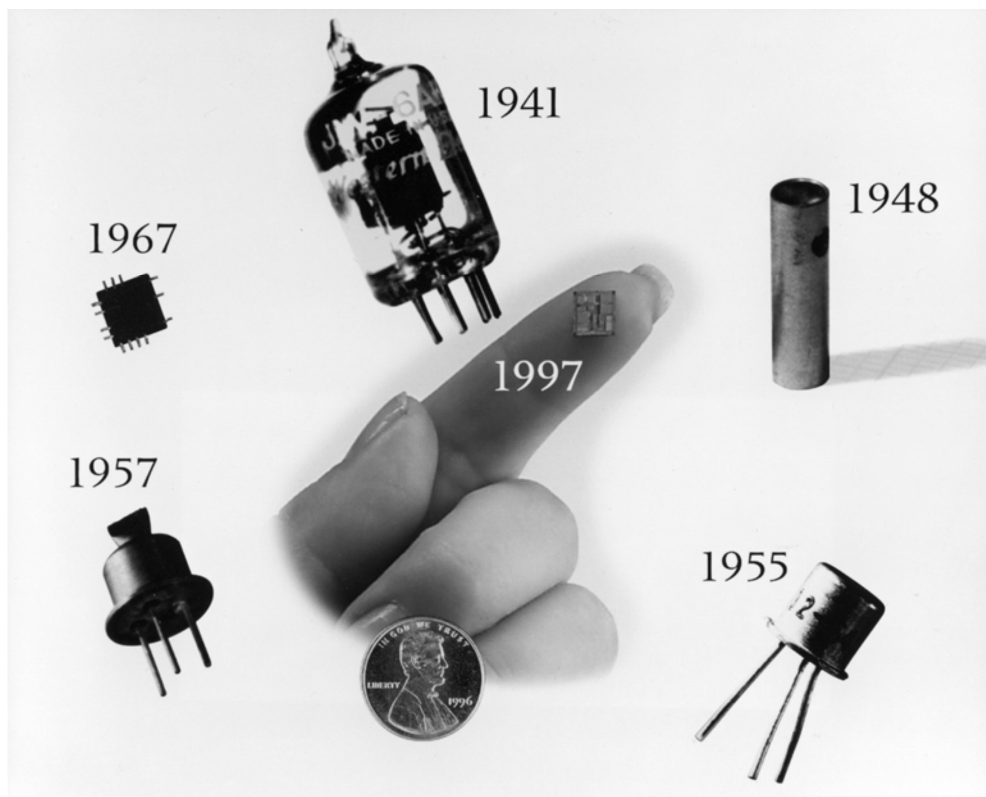

(b)

Figure 1.1: (a) A replica of the first working transistor (b) Transistor and Integrated Circuits (ICs) chronology [Source: Bell Labs].

they never referenced this work in any of their research papers or historical articles [2]. Bardeen, Brattain and Shockley were awarded the Nobel Prize in physics in 1956. The first silicon transistor was produced by Texas Instruments in 1954. This was the work of Gordon Teal, an expert in growing crystals of high purity, who had previously worked at Bell Labs. The first MOS transistor actually built was by Kahng and Atalla at Bell Labs in 1960 [3].

1.2 REVIEW OF RECENT WORK

Several analytical work have been reported on the base transit time for low and high levels of injection in the base. Moll and Ross [4] formulated a double integral relation of transit time for a homojunction bipolar transistor. The proposed expression is given below

$$\tau_B = \frac{1}{D_n}\int_B \frac{1}{N_B}\left[\int_x^{W_B} N_B dy\right]dx \tag{1.1}$$

In this model, the base transit time depends on the base doping (here acceptor) concentration (N_B) and the minority carrier (here electron) diffusivity (D_n) and it is only applicable for low level of injection.

J. J. H. Van den Biesen [5] in 1986 studied the base transit time of a bipolar junction transistor using regional analysis by means of a numerical device simulation program for high level of injection. He used an expression for base transit time based on perturbation theory and that was written as

$$\tau_B = q\int_{x_E}^{x_C} \left|dn/dJ_c\right|_{v_{ce}=0} dx \tag{1.2}$$

K. Suzuki and N. Nakayama [6] in 1992 derived an analytical expression for the base transit time considering carrier velocity saturation at base-collector junction. The derived equation is

$$\begin{aligned}\tau_B &= \int_0^{W_B} \frac{n_{ie}^2(x)}{N_B(x)}\left\{\int_x^{W_B} \frac{1}{D_n(y)}\frac{N_B(y)}{n_{ie}^2(y)}dy\right\}dx + \frac{1}{v_s}\frac{N_B(W_B)}{n_{ie}^2(W_B)}\int_0^{W_B}\frac{n_{ie}^2(x)}{N_B(x)}dx \\ &= \frac{W_B^2}{k_1 D_n(0)} + \frac{W_B}{k_2 v_s}\end{aligned} \tag{1.3}$$

where, $$k_1 = \frac{W_B^2}{\int_0^{W_B} \frac{n_{ie}^2(x)}{N_B(x)} \int_x^{W_B} \frac{1}{D_n(y)} \frac{N_B(y)}{n_{ie}^2(y)} dy dx} \tag{1.4}$$

$$k_2 = \frac{W_B}{\int_0^{W_B} \frac{N_B(W_B)}{n_{ie}^2(W_B)} \frac{n_{ie}^2(x)}{N_B(x)} dx} \tag{1.5}$$

here n_{ie} is the intrinsic carrier concentration, v_s is the saturation velocity of electron. This analysis was done only for low injection region.

In 1996, M. M. Jahan and A. F. M. Anwar [7] modified the double integral relation of transit time for exponentially doped base, which can be applicable both for homojunction and heterojunction bipolar transistors. This model included doping dependent mobility variation, bandgap narrowing and finite velocity saturation effects in the calculation of base transit time but ignored the electric field dependency of mobility and avoided high injection region of operation.

In 1997, N. Rinaldi [8] presented an analytical model for base transit time with an exponentially doped base BJT. This model included dependence of the mobility on doping concentration and electric field, heavy-doping effects and finite carrier velocity at the collector edge. This model is also applicable to HBT with a linearly graded Ge composition. Other forms of Ge composition variation (e.g. box, trapezoidal) are not addressed in Rinaldi's model and it is only valid for low level of injection and the analytical expression for base transit time is quite long as given below

$$\tau_B = \left[\tau_{B0}^{\gamma} + \left(\frac{W_B}{\eta_R v_s} \left(\eta_R - 1 + e^{-\eta_R} \right) \right)^{\gamma} \right]^{1/\gamma} + \frac{W_B}{S} \frac{1 - e^{-\eta_R}}{\eta_R} \tag{1.6a}$$

and $$\tau_{B0} = \left(\frac{W_B}{\eta_R} \right)^2 \frac{\eta_R - 1 + e^{-\eta_R}}{D_{\max}} + \left(\frac{W_B}{\eta_R} \right)^2 \frac{\left(N_B(W_B)/N_r \right)^{\gamma_m}}{D_{\max} \left(1 + \gamma_m \eta / \eta_R \right)} \left[\frac{\eta_R}{\gamma_m \eta} \left(e^{\gamma_m \eta} - 1 \right) - 1 + e^{-\eta_R} \right]$$

(1.6b)

where γ is a constant with value of 1 or 2, v_s is the saturation velocity of electron, S is the velocity of electron (without saturation), $D_{\max}$ is the maximum value of diffusivity, $N_r = 10^{17}$ cm^{-3}, $\gamma_m = 0.468$, $\eta_R = \eta_2 + \eta_E$, $\eta_2 = \eta(1-\gamma_2)$, η is the slope of base doping, $\gamma_2 = 0.69$, $\eta_E = (\Delta E^C_G(W_B) - \Delta E^C_G(0))/kT$, ΔE^C_G is the conduction band energy gap.

In 1998, V. S. Patri and M. J. Kumar [9] developed a unified closed form analytical model for base transit time of SiGe HBT's for uniform and exponential base doping with different Ge profiles in the base (e.g. box, trapezoidal, triangular) while taking into consideration doping induced bandgap narrowing and diffusion coefficient. The model avoided high injection region of operation and field dependent mobility. The analytical form is also complicated and difficult to get a complete picture.

K. H. Kwok [10] in 1999 used a regional base transit time model which results in a set of closed-form analytical expressions for an exponentially-doped retrograde base of a SiGe-base HBT with a linearly graded Ge profile. This model considered the retarding built-in electric field due to the retrograde region, heavy doping effects, the effect of velocity saturation at the base-collector junction, the effects of the doping dependency and the electric-field dependency of the electron diffusivity and the electric field induced by the Ge concentration gradient. However, this model was not valid for high level of injection and the analytical expressions for regional base transit time were very long and complicated.

M. M. S. Hassan and A. H. Khondoker in 2001 [11] derived a new mathematical expressions for electron current density and base transit time for uniform base doping profile of a BJT for all levels of injection. This model did not use Moll's double integral form of base transit time. In this work base doping density dependence of mobility was considered but the carrier saturation velocity and electric field dependent mobility was neglected. It is also noteworthy that in practical transistor the base is not uniformly doped. In practical transistor base doping follows Gaussian distribution [12]. G. Li *et al.* in their 2001 work [12] showed that a Gaussian profile can be well approximated by a simple exponential profile. M. Z. R. Khan *et al.* [13], F. M. Mohammedy *et al.* [14], M. A. Abedin *et al.* [15], T. Rahman *et al.* [16] and M. W. K. Nomani *et al.* [17] used nonuniformly doped base profile for the modeling of base transit time.

K. H. Kwok and C. R. Selvakumar [18] in 2001 reported a work on base transit time for all levels of injection before onset of Kirk effect. They solved the equations

numerically using iterative techniques to show different effects of base doping and Ge profiles on base transit time.

A number of studies have been found in literatures on the base transit time of SiGe base HBTs. S. T. Chang *et al.* [19], S. K. Mandal *et al.* [55] in 2004, M. K. Das *et al.* [20] in 2005, S. Basu [21] in 2008 have reported on transit time and high frequency performance of SiGe HBT but none of these works has modeled the high level of injection. Up to recent time, a very few number of analytical models of base transit time for HBT have addressed the electric field dependency of minority carrier mobility and none of them have dealt with high level of injection.

However, for BJT a number of studies have been found in the literature searching for suitable analytical expressions of base transit time for high level of injection. K. Suzuki [22] in 1994, P. Ma *et al.* [23] in 1998 and M. M. S. Hassan *et al.* [24] in 2006 used perturbation theory to model base transit time for all levels of injection. Suzuki's model ignored filed dependent mobility, P. Ma used iterative method and M. M. S. Hassan considered filed dependent mobility. Yeasir Arafat *et al.* [25] presented calculation of base transit time for exponentially doped base considering both doping and electric field dependency of mobility, velocity saturation at the collector-base junction etc. A. Zareba *et al.* [26] presented calculation of selected parameters of SiGe HBT with Gaussian doping using numerical techniques.

1.3 SCOPE OF THIS DISSERTATION

The main objective of this work is to obtain an analytical expression for base transit time of an n^+-p-n $Si_{1-y}Ge_y$ base HBT with nonuniform base doping distribution (Gaussian doping) and three different type of Ge profiles (e.g. box, trapezoidal, triangular) for low and moderate levels of injection considering electric field dependent mobility. Model development will be based on the formulation of Yeasir Araftat *et. al.* [25], who calculated base transit time assuming exponential base doping. In the proposed work, perturbation theory along with Webster effect will be used to model base transit time for

Gaussian doped base in place of exponential doping. Effect of doping dependent mobility, bandgap narrowing, carrier velocity saturation etc. will be considered. The injected minority carrier, collector current density, stored base charge, electric field in the base will be studied as well. It is expected that the derived model will give prompt and precise base transit time for realistic transistors. Numerical results obtained by this model will be compared with numerical data available in the literature.

1.4 CHAPTER LAYOUT

In this work the expressions for injected minority carrier concentration profile, collector current density and hence the base transit time of a heterojunction bipolar transistor are derived. In chapter one previous works on base transit time have been reviewed and the justification of carrying out the research is given. Mathematical analyses are given in chapter two. In chapter three the dependence of current and base transit time on various device parameters are studied. The transit time obtained from the derived equation is compared to that of numerical analysis in order to demonstrate the validity of the assumptions made in deriving expression for base transit time. Finally this dissertation ends in chapter four containing salient features of this work and possible future field of studies.

CHAPTER 2

BACKGROUND

2.1 TRANSISTOR CATEGORIES

After the success of Bell Labs, many other organizations came ahead and invested hugely in the research of solid-state electronics. The outcome was tremendous in the next few years as this has instigated a new era called ‘electronic age’ and till date solid-state electronics research leads the world market based on scientific research. By this long span of time, various forms of transistors have been modeled, patented and experimented. A few of them are categorized here in the following table.

Table 2.1: Different type of Transistors (adapted from [27])

Based on	**Category**	
Structure	Junction Transistor (Bipolar Transistor)	BJT (Bipolar Junction Transistor) HBT (Heterojunction Bipolar Transistor) Insulated Gate Bipolar Transistor (IGBT)
	Field Effect Transistor (Unipolar Transistor)	Junction Field Effect Transistor (JFET) Metal Oxide Semiconductor FET (MOSFET or IGFET)
Polarity		BJT: *npn*, *pnp*
		FET: *n*-channel, *p*-channel
Material		Germanium (Ge), Silicon (Si), Gallium Arsenide (GaAs), Indium Phosphide (InP), Silicon Carbide (SiC) etc.
Power rating		Low, medium, high
Frequency		Radio frequency (RF), microwave etc.
Application		Switch, audio, high voltage, super-beta, matched pair etc.
Packaging		Through hole metal or plastic, surface mount, ball grid array etc.

2.2 BIPOLAR TRANSISTOR

A bipolar transistor takes shape as the doping of a semiconductor proceeds. The process of adding controlled impurities into the crystal lattice of a semiconductor is known as doping. The amount of impurity (dopant) added to an intrinsic semiconductor varies its level of conductivity. Doped semiconductors are often referred to as extrinsic. By adding impurity to intrinsic semiconductors, the electrical conductivity may be varied not only by the number of impurity atoms but also, by the type of impurity atom and the changes may be thousand folds and million folds. For example- 1 cm^3 of a metal or semiconductor specimen has a number of atoms on the order of 10^{22}. Since every atom in metal donates at least one free electron for conduction in metal, 1 cm^3 of metal contains free electrons on the order of 10^{22}. At the temperature close to 20 °C, 1 cm^3 of intrinsic germanium contains about 4.2×10^{22} atoms and 2.5×10^{13} free electrons & 2.5×10^{13} holes. The addition of 0.001% of arsenic donates an extra 10^{17} free electrons in the same volume and the electrical conductivity increases about 10,000 times [28].

2.2.1 Dopants

Dopants are classified as either electron acceptors or donors. A donor atom donates weakly-bound valence electrons to the material, creating excess negative charge carriers. These weakly-bound electrons can move about in the crystal lattice relatively freely and can facilitate conduction in the presence of an electric field. Conversely, an activated acceptor produces a hole. Semiconductors doped with donor impurities are called *n*-type, while those doped with acceptor impurities are known as *p*-type. The *n* and *p* type designations indicate which charge carrier acts as the material's majority carrier. The opposite carrier is called the minority carrier, which exists due to thermal excitation at a much lower concentration compared to the majority carrier.

Intrinsic Si has 4 valence electrons. In Si, the most common dopants are group III & group V elements. Group III (boron(B:2,3), aluminum(Al:2,8,3), gallium(Ga:2,8,18,3), indium(In:2,8,18,18,3) and thallium(Tl:2,8,18,32,18,3)) all contain three valence electrons, causing them to function as acceptors when used to dope Si. Group V elements

(nitrogen(N:2,5), phosphorus(P:2,8,5), arsenic(As:2,8,18,5), antimony(Sb:2,8,18,18,5) & bismuth(Bi:2,8,18,32,18,5)) have 5 valence electrons, which allow them to act as a donor.

The number of dopant atoms needed to create a difference in the ability of a semiconductor to conduct is very small. When a comparatively small number of dopant atoms are added on the order of one per 100 million atoms, the doping is said to be low or light. When many more dopant atoms are added on the order of one per ten thousand atoms, the doping is referred to as heavy or high. This is often mentioned as n^+ for *n*-type doping or p^+ for *p*-type doping. When a semiconductor is doped to such high level, it acts almost like a conductor and is referred as a degenerate semiconductor [28].

2.2.2 Doping process

Some dopants are added as (usually) the silicon boule is grown using the Bridgeman technique or the Czochralski process, giving each wafer an almost uniform initial doping. For desired device properties, selected areas typically controlled by photolithography are further doped by such processes as diffusion and ion implantation. The latter method being more popular in large production runs because of increased controllability. The molecular beam epitaxy (MBE) or chemical vapor deposition (CVD) technologies are also used in transistor manufacturing where precisely controlled doping is required [29].

2.2.3 The n^+-*p*-*n* transistor

An *n-p-n* bipolar junction transistor consists of two back-to-back *p-n* junctions, who share a thin common region. Metal contacts are made to all three regions. The operation of a bipolar junction transistor depends on the forward and the reverse current of the two back-to-back *p-n* junctions. The forward-biased junction, which injects electrons into the center *p* region, is called base-emitter junction and the reversed-biased junction, which collects the injected electrons, is called the base-collector junction. The region, which serves as the source of injected electrons, is called the emitter and the *n* region into which electrons are swept by the reverse-biased junction is called the collector. The center region is called the base.

For practical interest, doping concentration of emitter is made very high. Thus it forms an n^+-p-n structure. Figure 2.2 shows the schematic diagram of an n^+-p-n bipolar junction transistor. To have a good n^+-p-n transistor, it is preferred that almost all the electrons injected by the emitter into the base be collected. Thus the p-type base region should be narrow. This requirement is summed up by specifying neutral base width should be less than the diffusion length of electron in the base. With this requirement satisfied, an average electron injected at the emitter junction will diffuse to the depletion region of the base-collector junction without recombination in the base. A second requirement is that the emitter current (I_E) crossing the emitter junction should be composed almost entirely of electrons injected into the base rather than holes crossing from base to emitter [30].

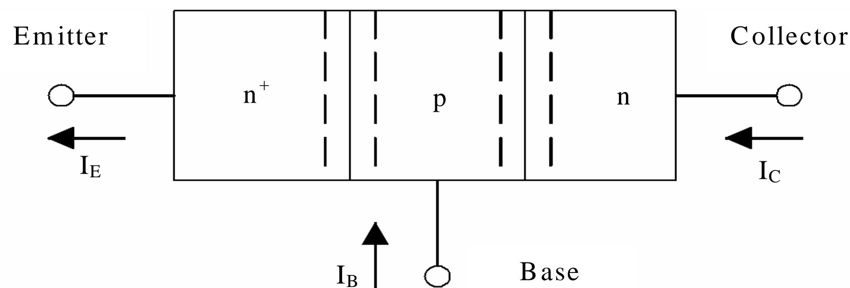

Figure 2.2: The schematic diagram of an n^+-p-n bipolar junction transistor. Conventional direction of current flow is assumed.

2.2.4 Suitability of bipolar transistor

Although Complimentary Metal Oxide Semiconductor (CMOS) transistor has acquired an ever-increasing role, the bipolar transistor retains its position as a technology of choice for high-speed circuits, ultra-high-frequency discrete logic circuits such as emitter coupled logic (ECL), power amplifiers in cellular phones, mixed-signal & precision analog components, microwave power amplifiers and in other applications like fiber-optic communication. The speed advantage (higher frequencies) together with trans-conductance (g_m), high current gain (β) and low $1/f$ noise continue to make the bipolar transistor the device of choice for many demanding applications [32]. One of the important figures of merit of BJTs is the transition frequency f_T[*], presently which ranges

[*] It is also called the unity current gain cutoff frequency; the theoretical frequency at which the short circuit current gain of the common-emitter (CE) mode transistor drops to 0 dB.

in the GHz level [28] and another important high frequency parameter is the maximum oscillation frequency f_{max} [†] which also ranges in the same level.

2.3 HETEROJUNCTION BIPOLAR TRANSISTOR

A heterojunction is the interface that occurs between two layers or regions of dissimilar crystalline semiconductors. These semiconductor materials have unequal band gaps as opposed to a homojunction. It is often advantageous to engineer the energy bands in many solid state devices. The *p-n* junctions in the Figure 2.2 are assumed to homojunction (same substrate is used for the emitter, base & collector). If different semiconductors were used as substrates for the emitter, base & collector, then the junctions would be termed as hetero junctions. With two hetero junctions, a bipolar transistor is identified as double heterojunction bipolar transistor (DHBT) or simply HBT. With one homojunction and another heterojunction, a bipolar transistor is termed as single heterojunction bipolar transistor (SHBT). Typically the emitter of the SHBT is wide bandgap material which allows heavy doping of the base for reduced base resistance while the emitter is more lightly doped reducing the capacitance and improving the high frequency performance. In the DHBT, the collector and emitter have wide bandgap materials allowing the same advantages of the SHBT, with the additional improvement of increased breakdown voltage and decreased minority carrier injection from the base to the collector in saturation mode [32].

So, the HBT is nothing but an improvement of the conventional BJT. Different semiconductor materials in the emitter and base prohibit the injection of electron from the emitter into the base region, since the potential barrier in the valence band is higher than in the conduction band. Unlike BJT, HBT technology allows a high doping density to be used in the base, reducing the base resistance while maintaining the gain. The idea of employing a heterojunction is as old as the BJT, dating back to a patent from 1951 [1]. Since then many scientists and engineers have contributed to the improvement of HBT and in the year 2000, the Nobel Prize in Physics was awarded with one half jointly to

[†] Also called the maximum power frequency and it is a function of f_T.

Herbert Kroemer and Zhores Alferov for "developing semiconductor heterostructure used in high-speed and opto-electronics" [33].

Different types of elements and compound semiconductor materials are used to fabricate heterojunction. HBTs are named after the materials used in substrate or in the epitaxial layers. Properties of material used determine the characteristics of HBTs and their costs. Table 2.2 shows a list of such common materials used to fabricate HBTs of different genres.

Table 2.2: Some common materials used for HBT (reproduced from [32])

Material Names	Symbols
Silicon/Silicon Germanium	Si/SiGe
Aluminum Gallium Arsenide/Gallium Arsenide	AlGaAs/GaAs
Indium Phosphide/Indium Gallium Arsenide	InP/InGaAs
Indium Aluminum Arsenide /Indium Gallium Arsenide	InAlAs/InGaAs
Aluminum Gallium Nitride/Gallium Nitride	AlGaN/GaN
Indium Gallium Phosphide/Gallium Arsenide	InGaP/GaAs
Indium Gallium Phosphide/Indium Gallium Arsenide Nitride	InGaP/InGaAsN

2.3.1 SiGe device physics

In SiGe devices, SiGe alloy is introduced into the base of a Si BJT by means of pseudomorphic growth of strained SiGe on Si. This process successfully utilizes bandgap engineering in the Si material system to achieve group III-V like performance while maintaining compatibility with conventional Silicon technology. From a performance perspective, introducing Ge into Si improves speed, current gain, noise characteristics and linearity. However, from a physical perspective, the difference in lattice constants between Ge and Si result in SiGe having a slightly higher lattice constant than Si. Ge has smaller bandgap energy than Si (0.66 eV and 1.12 eV respectively); consequently SiGe has a smaller bandgap than Si facilitating bandgap engineering in Si.

The compressive strain in the SiGe film produces an additional bandgap shrinkage resulting in about 75meV reduction in bandgap for every 10% of Ge introduced. Since this “band offset” occurs primarily in the valence band, *n-p-n* Si BJTs can be tailored to obtain required performance metrics. The compressive strain also lifts the conduction and

valence band degeneracies at the band extremes. This effectively reduces the density of states (DOS) and improves carrier mobilities.

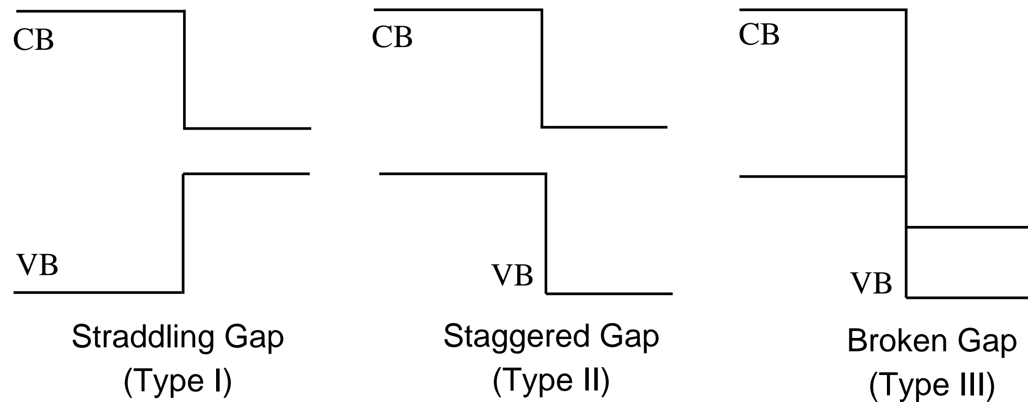

Figure 2.3: The three types of semiconductor heterojunctions organized by band alignment. Here CB stands for conduction band and VB is the valence band.

The presence of Si/SiGe heterojunction in the emitter-base (EB) and base-collector (BC) junctions of the HBT results in a marked performance improvement in both dc and ac characteristics over the Si BJT. The energy band diagrams of a forward biased graded-base SiGe HBT and a Si BJT are shown in Figure 2.4.

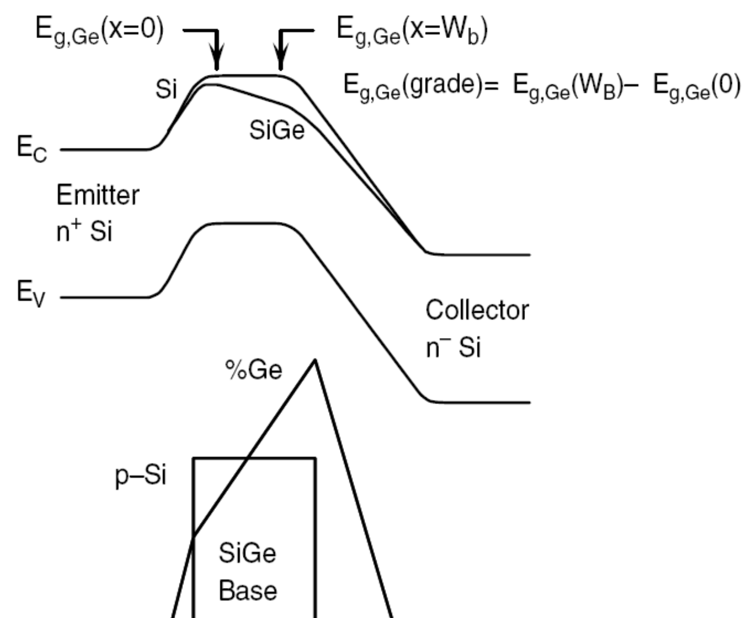

Figure 2.4: Energy band diagram for a graded base SiGe HBT and a Si BJT, biased in forward active mode at low-injection (reproduced from [34]).

The effect of graded Ge content in the base on the band structures is perceptible from the Figure 2.4.

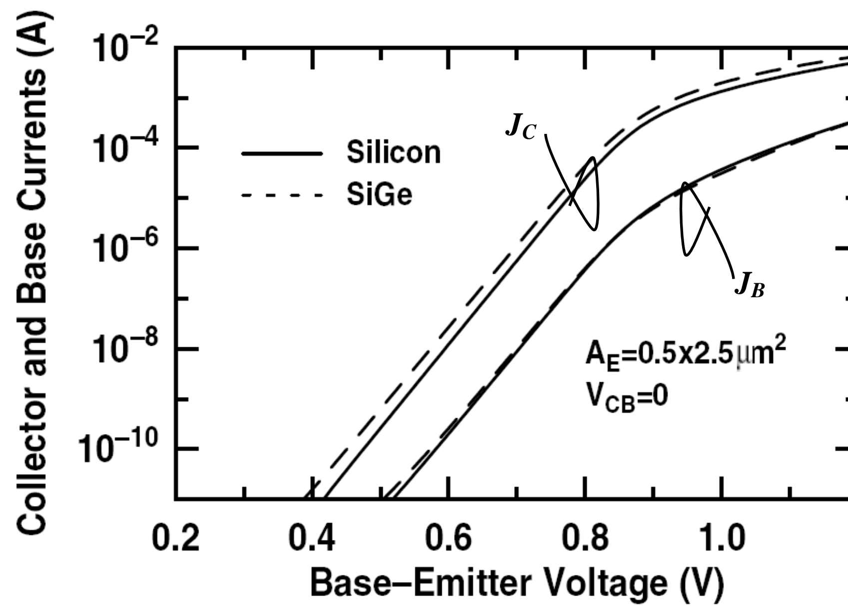

(a)

Figure 2.5: Representative Gummel characteristics for a typical SiGe HBT and a similarly constructed Si BJT (reproduced from [34]).

A slight reduction in the base bandgap at the EB junction ($\Delta E_{g,Ge}(x=0)$) and a much larger reduction at the BC junction ($\Delta E_{g,Ge}(x=W_B)$) is observed. This grading of Ge mole fraction across the base induces a built-in quasi-drift field $(((\Delta E_{g,Ge}(x=W_B))-(\Delta E_{g,Ge}(x=0)))/W_B)$ in the neutral base region, positively impacting the minority carrier transport. From Figure 2.4, it is seen that the emitter-base potential barrier is reduced in the SiGe HBT with respect to the Si BJT, thereby allowing increased electron injection from emitter to base. The enhanced electron injection leads to a higher collector current and current gain.

Figure 2.5 depicts the Gummel plot for a SiGe HBT as compared to a Si BJT. As expected, the SiGe HBT exhibits higher collector (J_C) current and approximately the same base current (J_B) as the Si BJT. The increase in J_C for the SiGe HBT in turn leads to an increase in current gain (β). The current gain depends linearly on the band offset due to Ge grading across the base and exponentially on the Ge induced band offset at the EB junction. Therefore, β is dependent on the Ge profile shape and can be modified for

particular circuit applications. The introduction of Ge in the base in effect decouples β from the base doping. This fact implies that the base doping can be increased with out degrading β. Note that higher base doping reduces the base resistance which has positive implications in terms of frequency response and broadband noise.

Other two important ac figures-of-merit are the transition frequency (f_T) and the maximum oscillation frequency (f_{max}). Ge content in the base has positive impacts on both these parameters. The transition frequency is given by [35]

$$f_T = \frac{1}{2\pi}\left[\tau_E + \tau_B + \frac{W_{BC}}{2v_s} + \left\{\left(C_{EB} + C_{BC}\right)\frac{1}{g_m} + R_C C_{BC}\right\}\right]^{-1} = \frac{1}{2\pi\tau_{EC}} \tag{2.1}$$

where τ_E is the emitter charge storage delay time, τ_B is the base transit time, W_{BC} is the width of base-collector space-charge layer, v_s is the saturation velocity, C_{EB} and C_{BC} are the emitter-base and base-collector depletion capacitances, g_m is the transconductance, R_C is the collector resistance and τ_{EC} is the total delay time from emitter to collector. The grading of Ge across the base induces a built-in electric field in the neutral base region (directed from collector to emitter). This field accelerates the minority carriers across the base which effectively reduces the base transit time. Due to the inverse relationship between the emitter charge storage delay time (τ_E) and current gain (β), the earlier is reduced as the later is higher for the SiGe HBT. Due to the reduction in τ_B and τ_E, f_T of the SiGe HBT increases over that of a Si BJT.

The maximum oscillation frequency of any bipolar transistor is given by [35]

$$f_{\max} = \sqrt{\frac{f_T}{8\pi R_B C_{BC}}} \tag{2.2}$$

where R_B is the ac base resistance which can be reduced by heavy doping in the base region using wide bandgap materials. It is quite evident from equation (2.2) that the maximum oscillation frequency (f_{max}) of the SiGe heterojunction bipolar transistor will experience a two fold increase once for its higher transition frequency and again for its lower base resistance.

2.3.2 SiGe HBT

In SiGe graded heterojunction transistors, the amount of germanium in the base is graded, making the bandgap narrower at the collector than at the emitter. That tapering of the bandgap leads to a field-assisted transport in the base, which speeds transport through the base and increases frequency response. Compared to silicon BJT, the SiGe HBTs have better device performance parameters (β, g_m and f_T). They satisfy the requirements of RF circuits such as modems, mixers, voltage controlled oscillators (VCOs), power amplifiers etc; mixed signal circuits like fractional N synthesizers & analog to digital converters and in the precision analog circuits such as Op-Amps, band gap references, temperature bias control and current mirrors etc [36]. Further, band gap engineering of SiGe facilitates in reducing forward voltage drop of the emitter-base junction by uniform grading at the emitter-base junction without affecting the other parameters [38] which makes it a best candidate for low voltage applications in wireless phones and other low power battery operated products. In addition to allowing very complex custom designs, high speed and high breakdown voltage SiGe HBTs can be merged with high density CMOS using a mixed signal methodology.

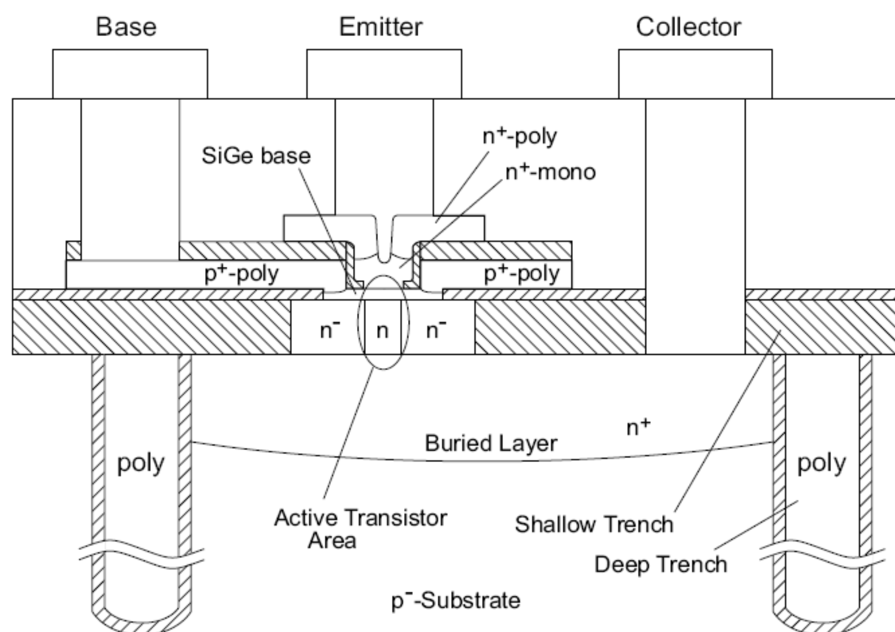

Figure 2.6: The schematic diagram showing the cross section of a SiGe heterojunction bipolar transistor.

Another prime aspect for a SiGe based HBT technology is the ability to merge the high performance SiGe HBT with standard CMOS technology giving rise to a high performance SiGe BiCMOS process without compromising the performance of either the HBT or the CMOS device. The combination of SiGe HBTs with scaled BiCMOS to form SiGe HBT BiCMOS technology presents an exciting possibility for system-on-chip (SoC) solution. Further, the use of SiGe devices allows many new functions to be added onto the silicon chip thus potentially reducing cost and power and increasing speed and yield. Ge ion implantation into Si has been successfully demonstrated to form SiGe [39]. But, it is difficult to obtain shallow junctions with sharp impurity profiles in vertical structures. However, recently it has been shown that this technique can be attractive for lateral SoI (Silicon on Insulator) HBT [39].

Key difference between SiGe HBTs & Si BJTs is the introduction of SiGe epitaxial layer into the base of an otherwise all-Si bipolar transistor. The base region is thus comprised of a Si buffer, boron-doped graded SiGe alloy active layer and a Si cap. Figure 2.6 depicts the schematic cross-section of a SiGe HBT while Figure 2.7 portrays Ge profile for a representative first generation SiGe HBT.

The SiGe HBT technology with 50 GHz (1st-generation) [40] and 120 GHz (2nd-generation) [41] peak cutoff frequency are currently in commercial production worldwide from multiple sources and are being deployed in both the commercial and defense sectors. The announcement of a third-generation SiGe HBT technology with 200 GHz peak cutoff frequency [42] and a fourth-generation SiGe HBT technology with over 300 GHz peak cutoff frequency [43], along with the complementary (*n-p-n* & *p-n-p*) SiGe HBTs with peak f_T values above 180 GHz and 80 GHz, respectively [44], have pushed the upper bound on the speeds achievable in these devices considerably higher than previously believed possible, thus vastly increasing the application options for SiGe HBT technology to encompass a wide variety of analog and RF through millimeter-wave systems [45]. While it might be argued that a peak cutoff frequency in excess of 200 GHz is not needed to support most IC applications, which are currently clustered in the 1-40 GHz range, such extreme levels of performance create a much broader circuit design space where, for instance, a designer has the option to trade frequency response for dramatic reductions in

power consumption (10x reduction in bias current in the third-generation devices over second-generation technology for similar operating speeds) [36].

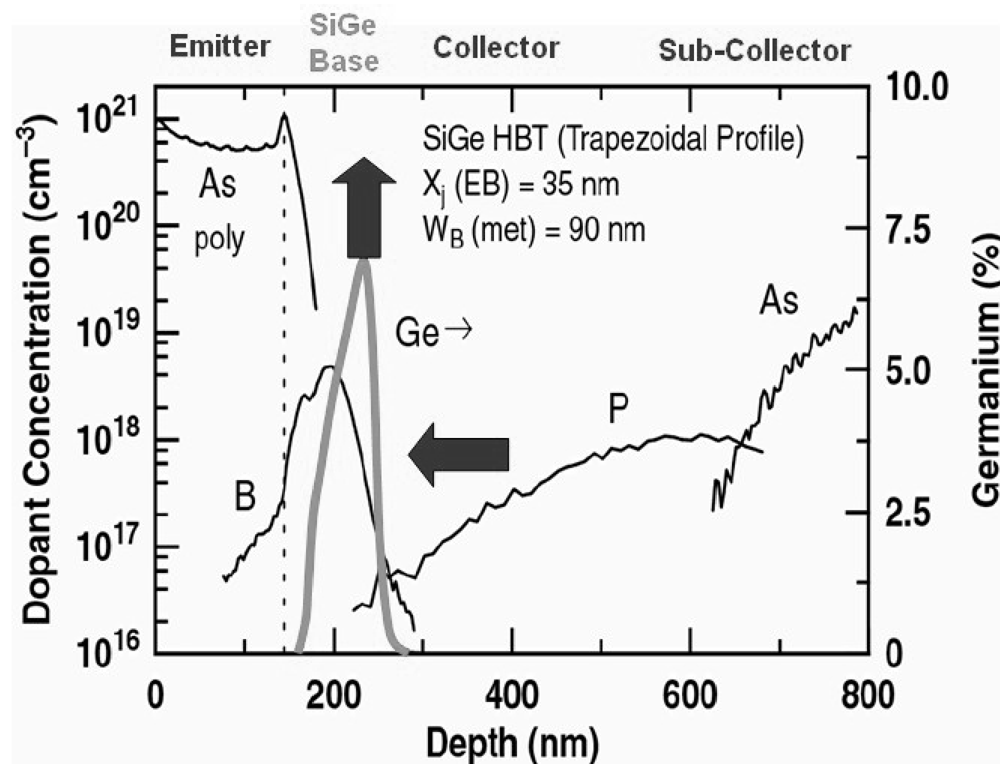

Figure 2.7: Representative base profiles for a first generation SiGe heterojunction bipolar transistor (reproduced from [34]).

2.3.3 Comparison between RFIC technologies

Gallium arsenide has historically been the preferred technology for power amplifiers used in RFIC because of its intrinsically higher low-field electron mobility (6 times higher than Si), transition frequency and breakdown voltage. The semi-insulating GaAs substrate also helps in developing high-Q passive elements. Due to higher bandgap energies and mobilities, GaAs power amplifiers have higher gain even at lower operating voltage. Even though GaAs has a number of advantages over Si, it also has some disadvantages which need to be considered. The thermal conductivity of GaAs is about 4 times lower than that of Si. This is a particularly difficult challenge for GaAs ICs as the power which must be dissipated is typically higher than that of Si ICs. Thermal management issue is a major consideration with regards to the ruggedness of the GaAs power amplifiers. Stability and reliability have also been areas of major concern in GaAs technology [46].

Recent advancements in Si-based RFICs, particularly the advent of SiGe HBTs, offer a significant challenge to GaAs HBT technology. The unity current gain cutoff frequency of SiGe HBT has reached a level comparable to GaAs technology. In fact SiGe HBT has been demonstrated with f_T beyond 500 GHz [47]. GaAs technology still has a significant performance advantage due to the higher low-field mobility which improves the minimum noise figure [48] but this is not a major concern in power amplifier design. SiGe technology also offers a potential cost advantage over GaAs due to compatibility with existing Silicon fabrication infrastructure. Finally, a high level of integration can be achieved in SiGe ICs which in turn reduces the packaging complexity.

A summary of the advantages of SiGe technology over other technologies is given below:

- Size and power consumption are critical for mobile applications. For a given f_T, a SiGe HBT would require only about a third of the collector current as compared to a Si BJT [49]. MOSFETs have lower g_m per mA as compared to BJT/HBT and the current required to obtain the same f_T for MOSFETs is larger [50].
- Breakdown voltages of SiGe HBTs are about twice those of Si BJTs for same f_T. As far as RF CMOS technology is concerned, the breakdown voltage as well as the maximum operating voltage are limited due to thin oxide breakdown and hot-carrier effects [51].
- HBTs have better noise performance since they have higher β and f_T as compared to BJTs. The base resistance of a SiGe HBT is lower than the Si BJT counterpart. CMOS devices have higher minimum noise figure as compared to bipolar devices when biased at the same current density [52].
- By optimizing the Ge profile in the base of a SiGe HBT, much higher Early voltage can be obtained than in BJTs. This results in higher r_o which maximizes gain and also helps in improving stability. The short-channel RF-MOSFETs have much lower r_o than SiGe HBTs due to increased channel-length modulation effects.
- HBTs have higher current gain than conventional BJTs as a result of which improved linearization by feedback is possible. Cancellation of the base-emitter heterojunction

capacitance improves the inter-modulation performance of HBT as compared to MESFET and HEMT. This results in excellent linearity data as reported in [53].

- Due to the advantages of SiGe HBT, such as higher current gain, early voltage, breakdown voltage and transit frequency, reduced base resistance as well as better transport properties of the base, performance approaching GaAs technologies can be achieved. Moreover, SiGe technology is currently being used to develop electronics for space applications due to their excellent analog and radio frequency performance over an extremely wide range of temperatures [54].

2.4 BASE TRANSIT TIME

When emitter-base junction of n^+-*p*-*n* transistor is forward biased, electrons from the emitter are injected in the base. Injected electrons are called minority carrier in *p*-type base. The average time taken by minority carriers to diffuse across the quasi-neutral base or the average time that an electron spends in the base is called the base transit time (τ_B). For an *n*-*p*-*n* HBT, the base transit time is given by [55]

$$\tau_B = \int_0^{W_B} \frac{qn(x)}{J_n(x)} dx \tag{2.3}$$

where, q is the charge of an electron, $n(x)$ is the minority carrier electron concentration within the base, J_n is the electron current density and W_B is the base width. If the recombination within the base is neglected then the electron current density becomes constant and eqn. (2.3) can be written as

$$\tau_B = \frac{1}{J_n} \int_0^{W_B} qn(x)dx = \frac{Q_{Bn}}{J_n} \tag{2.4}$$

and

$$Q_{Bn} = q \int_0^{W_B} n(x)dx \tag{2.5}$$

where, Q_{Bn} is the stored base charge per unit area.

Among different delay terms in (2.1), the base transit time is one of the most dominant factors in deciding f_T. The base transit time is more than 70% of a

heterojunction bipolar transistor's total delay time [56]. So, the base transit time plays a very crucial role in determining a transistor's high frequency performance. It is of great importance to obtain an accurate yet relatively simple analytical model of collector current density and base transit time for efficient device design.

The base transit time of a SiGe HBT is influenced by many physical and electrical parameters and various other factors such as

- Base width
- Various doping concentration profiles in the base region (uniform, linear, exponential, Gaussian, retrograde & complementary effort function)
- Various Ge profiles in the base region (box, triangular, trapezoidal)
- Velocity saturation effect
- Collector current density
- Built-in electric field in the base region
- Electric field and doping dependent carrier mobility
- Bandgap narrowing
- Base resistance etc.

CHAPTER 3

MATHEMATICAL ANALYSIS

3.1 INTRODUCTION

Calculation of base transit time for HBT with non-uniform base doping is an important issue. Before calculation of transit time, one should consider: (a) various Ge profiles with non-uniformly doped base (b) change in Ge dose and gradient (c) heavy doping or band gap narrowing effect (d) finite carrier velocity at the collector edge (e) dependence of mobility on electric field and doping concentration (f) high injection effects. Calculation of base transit time with Gaussian base doping $Si_{1-y}Ge_y$ n^+-p-n HBT is provided in this chapter considering all the above-mentioned effects. The injected minority carrier concentration profile $n(x)$ and collector current density J_c is modeled and calculated for moderate level of injection. The derivation of the model equation starts by first considering low level of minority carrier injection within the base. Then the minority carrier profile of low level of injection is extended for finding minority carrier profile for moderate level of injection using Perturbation Theory [22-24] and Webster effect [57]. To achieve this, current continuity equation, electric field equation, expression for field and doping dependent mobility and effective intrinsic carrier concentration for high base doping were deduced. It is assumed that for moderate level of injection, $n(x)$ is perturbed by the electric field from the modified low injection profile only a small amount $\delta n(x)$. Incorporating this small change in the current density equation, the differential equation for minority carrier concentration $n(x)$ is solved. Once $n(x)$ is known, the analytical expressions for J_n, Q_{Bn} and τ_B can easily be obtained.

3.2 DERIVATION OF MODEL EQUATIONS

The Ge mole fraction (y) distribution profiles of an n^+-p-n $Si_{1-y}Ge_y$-base HBT is shown in Figure 3.1. For a generalized trapezoidal profile, Ge mole fraction can be expressed as a function of distance along the base

$$y(x) = m_{Ge}x + y_E \tag{3.1}$$

where, x is the distance of a point in the base measured from the emitter-base (EB) junction of the HBT, $m_{Ge} = (yc-ye)/W_B$, W_B is the neutral base width, y_C and y_E are Ge fractions at the collector and emitter end of the base respectively. For $y_E = 0$, (3.1) represents triangular profile, for $y_E = y_C$, (3.1) represents box shape Ge profile [58]. Total Ge content within the base termed as "Ge dose" is calculated as [18]

$$y_D = y_{av}W_B \tag{3.2}$$

where,
$$y_{av} = (y_C + y_E)/2 \tag{3.3}$$

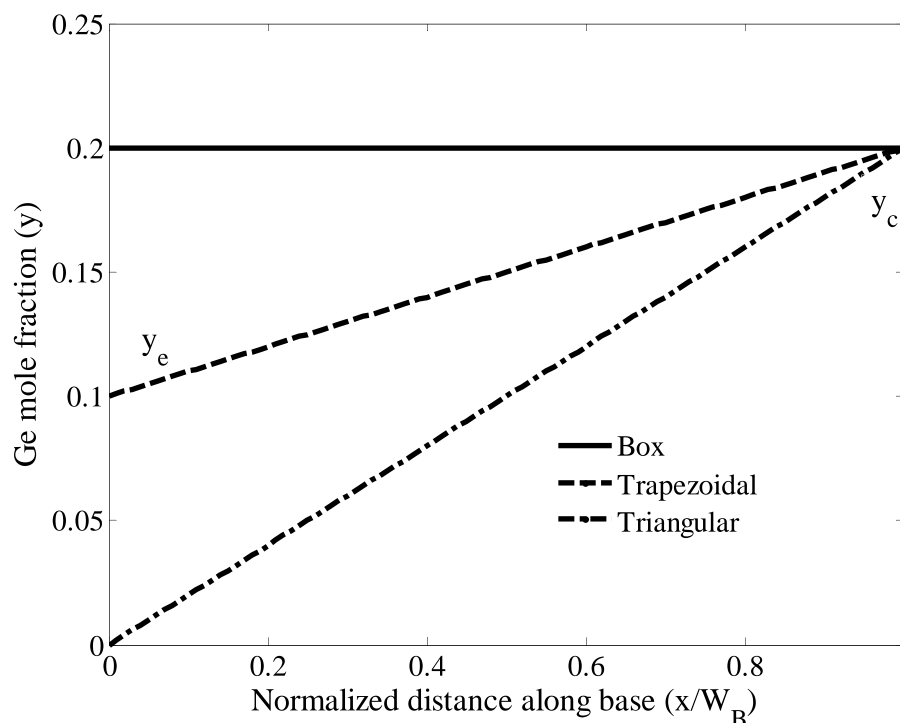

Figure 3.1: Ge mole fraction distribution within the base of a $Si_{1-y}Ge_y$ HBT for various geometric profiles.

The schematic representation of an n^+-p-n transistor is shown in Figure 3.2. The electron current density J_n and hole current density J_p with arbitrary base doping concentration $N_B(x)$ are given by the transport equations [59-60]

$$-J_n(x) = q\,D_n(x)\frac{dn(x)}{dx} + q\,\mu_n(x)n(x)E(x) \quad (3.4a)$$

$$J_p(x) = -q\,D_p(x)\frac{dp(x)}{dx} + q\,\mu_p(x)p(x)E(x) \quad (3.4b)$$

where, $D_n(x)$ & $D_p(x)$ are the diffusion co-efficient (or diffusivity) for electron & hole, $\mu_n(x)$ & $\mu_p(x)$ are the electron & hole mobility, $n(x)$ & $p(x)$ are the electron & hole concentration respectively and $E(x)$ is the electric field at a point x within the base. The direction of J_n in (3.4a) is defined such that it has a positive value. The total current density is the sum of the electron and hole current density.

$$J_c(x) = J_n(x) + J_p(x) \quad (3.5)$$

The electron diffusion length in silicon is about 500nm even at doping concentration as high as 10^{20} cm^{-3} [61]. As the base width of a modern high-speed HBT is very thin (less than 100nm even 26nm base width is reported in [18]), the carrier recombination in the base region can safely be neglected. So,

$$J_p(x) = 0 \quad (3.6a)$$

and $$J_c(x) \cong J_n(x) \quad (3.6b)$$

Therefore, the minority carrier current density J_n within the base becomes constant and is equal to collector current density J_c. In the present work, minority carrier concentration at thermal equilibrium has been neglected.

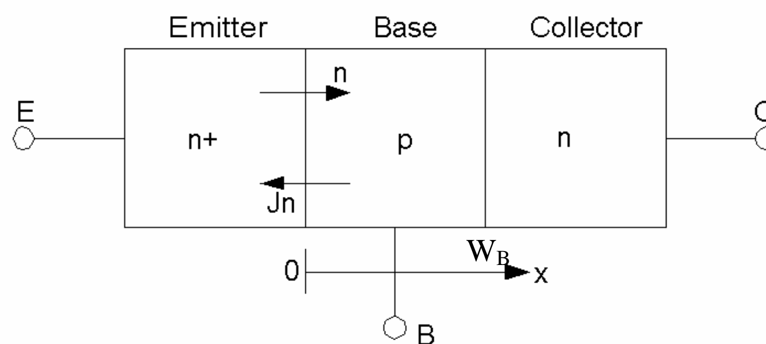

Figure 3.2: One-dimensional view of an *npn* SiGe heterojunction bipolar transistor showing flow of injected minority carrier and current density.

The electric field neglecting recombination in the base and considering band gap narrowing effect is [18, 62]

$$E(x)=V_T\frac{d}{dx}\left[\ln\left(\frac{p(x)}{n_{ie}^2(x)}\right)\right] \tag{3.7a}$$

where, V_T is the thermal voltage and is equal to kT/q, k is the Boltzmann constant, T is the temperature in degrees Kelvin, $n_{ie}(x)$ is the effective intrinsic carrier concentration in the base.

Equation (3.7a) can be written as follows [59]

$$E(x)=V_T\left(\frac{1}{p(x)}\frac{dp(x)}{dx}-\frac{1}{n_{ie}^2(x)}\frac{dn_{ie}^2(x)}{dx}\right) \tag{3.7b}$$

The first term in (3.7b) represents electric field due to concentration gradient and the second term in (3.7b) represents the quasi-field due to nonuniform band gap narrowing. Carrier mobility and diffusivity are correlated as described by the Einstein's relation [62]

$$D_n(x)=V_T\mu_n(x) \tag{3.8}$$

The quasi-neutrality of charge within the base of a bipolar transistor is [63]

$$p(x)=n(x)+N_B(x) \tag{3.9}$$

Using (3.4a) and (3.7-3.9), the minority carrier current density equation can be written as

$$-J_n=qD_n(x)\frac{n_{ie}^2(x)}{n(x)+N_B(x)}\frac{d}{dx}\left[\frac{n(x)\{n(x)+N_B(x)\}}{n_{ie}^2(x)}\right] \tag{3.10}$$

Equation (3.10) can be solved for $n(x)$ to find out the current density J_n and stored base charge per unit area Q_{Bn}.

Base doping distribution used in this analysis is assumed to be Gaussian [59]. The Gaussian distribution is given by,

$$N_B(x)=N_B(0)\exp\left(-mx^2\right) \tag{3.11}$$

where, $N_B(0)$ is the peak base doping concentration, $m=\frac{1}{2\sigma^2}$ and $\sigma=\frac{W_B}{\sqrt{2\ln\frac{N_B(0)}{N_B(W_B)}}}$ controls the slope of base doping.

The effective intrinsic carrier concentration $n_{ie}(x)$ is a function of the base doping concentration $N_B(x)$ through bandgap narrowing effect. For large electric field, the carrier mobility turns out to be a function of electric field as well as doping density [24]. The low

field doping density dependent electron diffusivity in Si, given in [60] can be rearranged as

$$D_{nSi}(x) = D_n \exp(m_1 x^2) \quad (3.12a)$$

where, $D_n = D_{n0}(N_B(0)/N_r)^{-\gamma}{}_1$, D_{n0}=20.72 cm^2/s, N_r=10^{17}cm^{-3}, $m_1 = m\gamma_1$ and γ_1=0.42. Here, γ_1 is a fit value. In the presence of Ge, the electron diffusivity is modified as [21]

$$D_{nSiGe}(x) = bD_{nSi}(x) \quad (3.12b)$$

where, b=1+3y_{av}.

The saturation velocity inside the SiGe alloy also differs from that in Si and is [19]

$$v_{sA} = cv_s \quad (3.13)$$

where, c=0.342/[0.342+y_{av}(1-y_{av})] and v_s=10^7 cm/s is the saturation velocity in Si.

The empirical expression for high field and doping dependent mobility in Si is [64]

$$\mu_{nSi}(|E|, x) = \frac{v_s}{a|E(x)| + E_{cSi}(x)} \quad (3.14a)$$

where, a=0.7743. $E_{cSi}(x)$ is the critical electric field and given by

$$E_{cSi}(x) = \frac{v_s}{\mu_{nSi}(x)} \quad (3.14b)$$

The effective intrinsic concentration in SiGe is [21]

$$n_{ieSiGe}^2(x) = n_{ioSi}^2 \gamma_r \exp\left(\frac{\Delta E_{geff}(x)}{kT}\right) \quad (3.15a)$$

where, n_{ioSi}=1.4x10^{10} cm^{-3} is intrinsic carrier concentration in undoped silicon, γ_r is the ratio of the effective density of states in SiGe to the effective density of states in Si as given in [62] and modified following [9]

$$\gamma_r = \exp\left(-\sqrt{5y_{av}}\right) \quad (3.15b)$$

$\Delta E_{geff}(x)$ is the effective bandgap reduction in the SiGe base that can be expressed as

$$\Delta E_{geff}(x) = \Delta E_{gHD}(x) + \Delta E_{gGe}(x) \quad (3.15c)$$

where $\Delta E_{gGe}(x)$ is the bandgap narrowing due to the presence of Ge which is assumed to have a linear dependence on Ge concentration, $\Delta E_{gHD}(x)$ is the bandgap narrowing due to heavy doping effects and is identical to that of Si [9]. An approximation of the Slotboom–de Graff bandgap narrowing model [65] is used for this term [66]

$$\Delta E_{gHD}(x) = qV_{gHD} \ln\left(\frac{N_B(x)}{N_r}\right) \tag{3.15d}$$

with, V_{gHD}=18 mV & the bandgap narrowing due to the presence of Ge is given by [55]

$$\Delta E_{gGe}(x) = qV_{gGe}\, y(x) \tag{3.15e}$$

with, V_{gGe}=688 mV. Combining (3.15a)-(3.15e), effective intrinsic concentration in SiGe can be expressed as

$$n_{ieSiGe}^2(x) = n_{ieSiGe}^2(0)\exp\left(m_3 x - m_2 x^2\right) \tag{3.15f}$$

where, $n_{ieSiGe}^2(0) = n_{ioSi}^2 \gamma_r \exp(\gamma_3 y_E)\left(\frac{N_B(0)}{N_r}\right)^{\gamma_2}$, $\gamma_2=V_{gHD}/V_T$ =0.69, $\gamma_3=V_{gGe}/V_T$, $m_2=m\gamma_2$, $m_3=m_{Ge}\gamma_3$.

It is required to obtain a mathematical expression for minority carrier concentration $n(x)$ and current density (J_n) in order to derive an expression for base transit time (τ_B). When the emitter-base junction is forward biased injected electron concentration depends on the externally applied voltage across base-emitter junction. The base will be subjected to three types of injection. At 'low injection', injected electron concentration will be much less than the doping concentration in the base, i.e. $n(x) \ll N_B(x)$. At 'strong high' level of injection, injected electron concentration will be much higher than the base doping concentration, i.e. $n(x) \gg N_B(x)$. But for moderate level of injection, the minority carrier concentration is comparable to the base doping concentration. Under this condition, neither $n(x)$ nor $N_B(x)$ can be ignored from the differential equation (3.10). As a result, (3.10) appears to be analytically intractable. But using perturbation theory and Webster effect simultaneously, $n(x)$ can be handled analytically a little bit further.

At first, fully closed form analytical expressions for minority carrier electron concentration, minority carrier current density, base stored charge and base transit time are obtained for low level of injection. Then this low-injection model is extended for moderate level of injection making a realistic assumption that the injected electron concentration $n(x)$ at moderate injection is perturbed by modulated electric field from its modified low injection solution $n_m(x)$ only a little amount $\delta_n(x)$. This technique gives a solution for minority carrier electron concentration $n(x)$. Applying velocity saturation at

the base-collector boundary under reverse bias condition, minority carrier current density J_n can be found from $n(x)$. Base stored charge Q_{Bn} is attained by integrating $n(x)$ over the base width and finally the base transit time can be obtained using (2.4).

3.2.1 Low injection model

For low injection, the quasi-neutral condition (3.9) becomes [24]

$$p_l(x) = n_l(x) + N_B(x) \approx N_B(x) \tag{3.16}$$

The subscript 'l' stands for low injection value of the associated parameter hereafter. From (3.7b) & (3.16), electric field distribution inside the base of a SiGe HBT becomes

$$E_{lSiGe}(x) = V_T\left(\frac{1}{N_B(x)}\frac{dN_B(x)}{dx} - \frac{1}{n_{ieSiGe}^2(x)}\frac{dn_{ieSiGe}^2(x)}{dx}\right) \tag{3.17a}$$

Using (3.11), (3.15f) and (3.17a), electric field under low injection becomes constant

$$E_{lSiGe}(x) = -V_T(m_3 + m_4 x) \tag{3.17b}$$

where, $m_4 = 2(m - m_2)$.

From (3.10) & (3.16), minority carrier current density (J_{nl}) of a SiGe HBT becomes

$$-J_{nl} = qD_{nSiGe}(x)\frac{n_{ieSiGe}^2(x)}{N_B(x)}\frac{d}{dx}\left[\frac{n_l(x)N_B(x)}{n_{ieSiGe}^2(x)}\right] \tag{3.18a}$$

Utilizing (3.11), (3.12b), (3.15f) and (3.18a) the following differential equation can be obtained

$$\frac{d}{dx}n_l(x) - n_l(x)(m_4 x + m_3) = -A_1 J_{nl} - A_2 x J_{nl} - A_3 J_{nl}\exp\left(-m_1 x^2\right) \tag{3.18b}$$

Where, $A_1 = \dfrac{am_3}{bqv_{sa}}$, $A_2 = \dfrac{am_4}{bqv_{sa}}$ and $A_3 = \dfrac{1}{bqD_n}$.

The solution of the differential equation (3.18b) is

$$n_l(x)\exp\left(-m_4\frac{x^2}{2} - m_3 x\right) - n_l(0) = -J_{nl}\int_0^x \exp\left(-m_4\frac{x^2}{2} - m_3 x\right)\left(A_1 + A_2 x + A_3\exp\left(-m_1 x^2\right)\right)dx$$

$$\Rightarrow n_l(x) = n_l(0)\exp\left(m_4\frac{x^2}{2} + m_3 x\right) - \exp\left(m_4\frac{x^2}{2} + m_3 x\right)J_{nl}\int_0^x \exp\left(-m_4\frac{x^2}{2} - m_3 x\right)\left(A_1 + A_2 x + A_3\exp\left(-m_1 x^2\right)\right)dx$$

Let,

$B_1(x)=\int_0^x A_1 \exp\left(-m_4\frac{x^2}{2}-m_3x\right)dx$, $B_2(x)=\int_0^x A_2 x\exp\left(-m_4\frac{x^2}{2}-m_3x\right)dx$ and

$B_3(x)=\int_0^x A_3 \exp\left(-\left(m_1+\frac{m_4}{2}\right)x^2-m_3x\right)dx$

Now, using integration tables/ Mathematica, we have,

$$B_1(x)=A_1\left[\sqrt{\pi}\frac{p_1}{m_3}\exp\left(p_1^2\right)\left\{erf\left(p_1+\frac{x}{\sqrt{2/m_4}}\right)-erf\left(p_1\right)\right\}\right], \quad \text{where, } p_1=\frac{m_3}{\sqrt{2m_4}}$$

$$B_2(x)=\frac{A_2}{m_4}\left[1-\exp\left(-m_3x-m_4\frac{x^2}{2}\right)-m_3\frac{B_1(x)}{A_1}\right]$$

$$B_3(x)=A_3\left[\sqrt{\pi}\frac{p_2}{m_3}\exp\left(p_2^2\right)\left\{erf\left(p_2+\frac{x}{\sqrt{2/(m_4+2m_1)}}\right)-erf\left(p_2\right)\right\}\right],$$

where, $p_2=\frac{m_3}{\sqrt{2m_4+4m_1}}$

Now putting these values in equation for $n_l(x)$, we get,

$$n_l(x)=\exp\left(m_4\frac{x^2}{2}+m_3x\right)\left(n_l(0)-J_{nl}\left(B_1(x)+B_2(x)+B_3(x)\right)\right) \quad (3.19)$$

where, $n_l(0)$ is the value of electron concentration at emitter-base (EB) junction (x=0), Assuming that the electron velocity reaching the base-collector (BC) depletion region (x=W_B) saturates at v_{sA}, the minority carrier current density becomes

$$J_{nl}=qv_{sA}\,n_l(W_B) \quad (3.20)$$

Using (3.19) and (3.20), electron concentration $n_l(W_B)$ at the BC junction can be written as

$$n_l(W_B)=\frac{n_l(0)\exp\left(m_4\frac{W_B{}^2}{2}+m_3W_B\right)}{1+qv_{sa}\exp\left(m_4\frac{W_B{}^2}{2}+m_3W_B\right)\left(B_1(W_B)+B_2(W_B)+B_3(W_B)\right)} \quad (3.21)$$

Integrating (3.19) over the base width, base stored charge per unit area can be obtained as

$$Q_{Bnl}=q\int_0^{W_B}n_l(x)dx \quad (3.22)$$

And the base transit time can be found by

$$\tau_{Bl}=\frac{Q_{Bnl}}{J_{nl}} \quad (3.23)$$

3.2.2 Model for moderate level of injection

The injected electron concentration $n(x)$ at moderate level of injection has been found not significantly changed from $n_l(x)$ for an exponentially-doped base BJT [24]. For $Si_{1-y}Ge_y$ HBT with Gaussian-doped base, the same is assumed and the hypothesis is validated by plotting modified minority carrier electron concentration profile $n_m(x)$ for an Gaussian doped base HBT and compared with numerically obtained $n(x)$ at moderate level of injection. The plot is given in Figure 3.3. Numerically obtained $n(x)$ is found not significantly different from $n_m(x)$.

For a given value of the base-emitter junction voltage V_{be}, the initial value of injected minority carrier concentration $n(0)$ is required for the calculation of final boundary value $n(W_B)$ and hence the minority current density J_n. The initial value $n(0)$ is obtained from the following relation [57, 68] with necessary modification for SiGe HBT

$$n(0) = \frac{n_{ieSiGe}^2(0)}{N_B(0)} \exp\left(\frac{V_{be}}{V_T}\right) f_w \tag{3.24a}$$

where,

$$f_w = \frac{1}{0.5 + \sqrt{0.25 + \frac{n_{ieSiGe}^2(0)}{N_B^2(0)} \exp\left(V_{be}/V_T\right)}} \tag{3.24b}$$

The modified injected electron concentration and current density, considering Webster effect [57] can be written as

$$n_m(x) = f_w n_l(x) \tag{3.25a}$$

$$J_{nm} = f_w J_{nl} \tag{3.25b}$$

Assume that the injected electron concentration $n(x)$ is perturbed by the modulated electric field from $n_m(x)$ only a little, which is [23]

$$n(x) = n_m(x) + \delta n(x) \tag{3.26a}$$

Using (3.9) and (3.26a), the quasi-neutrality of charge equation can be written as

$$p(x) = n_m(x) + \delta n(x) + N_B\left(x\right) = p_m(x) + \delta n(x) \tag{3.26b}$$

Equating the middle and right parts of (3.26b), the following equation can be obtained

$$p_m(x) = n_m(x) + N_B\left(x\right) \tag{3.26c}$$

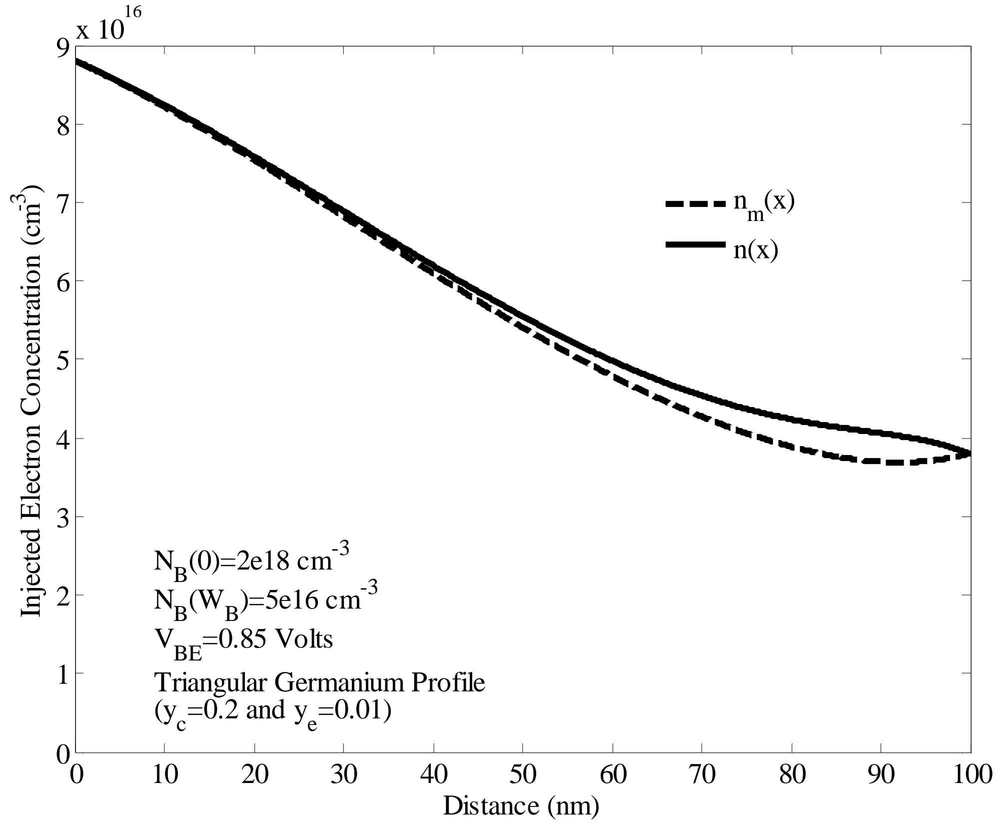

Figure 3.3: Comparison of injected minority carrier profiles within the base of a $Si_{1-y}Ge_y$ HBT modified from the low injection model ($n_m(x)$) and obtained from numerical solution under moderate injection ($n(x)$). Doping and field dependent mobility is considered.

From (3.10) & (3.26a-c), minority carrier current density J_n of a SiGe HBT becomes

$$-J_n = qD_{nSiGe}(x)\frac{n_{ieSiGe}^2(x)}{p_m(x)+\delta n(x)}\frac{d}{dx}\left[\frac{\{n_m(x)+\delta n(x)\}\{p_m(x)+\delta n(x)\}}{n_{ieSiGe}^2(x)}\right] \tag{3.27a}$$

To ensure the accuracy of the derivation, the magnitude of $\delta_n(x)$ must be much smaller than $p_m(x)$ instead of $n_m(x)$. Incorporating this assumption into (3.27a), the current density equation reduces to

$$-J_n = qD_{nSiGe}(x)\frac{n_{ieSiGe}^2(x)}{p_m(x)}\frac{d}{dx}\left(\frac{n(x)p_m(x)}{n_{ieSiGe}^2(x)}\right) \tag{3.27b}$$

Equation (3.27b) is a first order differential equation for $n(x)$. Utilizing (3.11), (3.12b), (3.15f), (3.25a) and (3.26a-c), the above differential equation can be solved for $n(x)$ as

$$n(x) = \frac{\exp\left(m_3 x - m_2 x^2\right)}{p_m(x)}\left(n(0)p_m(0) + \frac{J_n}{qv_{sa}}N(x)\right) \tag{3.28}$$

where

$$N(x) = \frac{a}{b} N_1(x) - \frac{v_{sa}}{bD_n} N_2(x)$$

$$N_1(x) = n_m(0)\{\exp(mx^2) - 1\} - J_{nm}\{B(x)\exp(mx^2) - B(0)\} + N_B(0)\left\{\exp\left(-\frac{m_4}{2}x^2 - m_3 x\right) - 1\right\}$$

$$N_2(x) = n_m(0)\{E_1(x) - E_1(0)\} - J_{nm}\{E_2(x) - E_2(0)\} + N_B(0)\{E_3(x) - E_3(0)\}$$

Applying velocity saturation at the base-collector depletion region, J_n can be written as

$$J_n = qv_{sA}\, n(W_B) \tag{3.29}$$

Substituting $x=W_B$ in (3.28) and using (3.29), $n(W_B)$ can be expressed as

$$n(W_B) = \frac{n(0)p_m(0)\exp\left(m_3 W_B - m_2 W_B{}^2\right)}{p_m(W_B) - N(W_B)\exp\left(m_3 W_B - m_2 W_B{}^2\right)} \tag{3.30}$$

The base stored charge per unit area for all levels of injection is

$$Q_{Bn} = q\int_0^{W_B} n(x)dx \tag{3.31}$$

The integration of the above base stored charge expression (3.31) is not analytically tractable. So, numerical methods have been used to find the base stored charge per unit area.

Now, the base transit time of a $Si_{1-y}Ge_y$ HBT with Gaussian (or uniformly) doped base and trapezoidal (or box/linear) Ge profile can be obtained for all levels of injection as

$$\tau_B = \frac{Q_{Bn}}{J_n} \tag{3.32}$$

3.3 CONCLUSION

In this chapter mathematical expressions for injected electron concentration profile $n(x)$, collector current density (J_n), stored base charge per unit area (Q_{Bn}) and hence the base transit time (τ_B) for an Gaussian doped $Si_{1-y}Ge_y$ n-p^+-n HBT are obtained considering all the effects especially dependence of mobility on electric field. The derivation of the model equation starts by first considering low level of minority carrier injection within the base. Then the minority carrier profile of low level of injection is extended for finding minority carrier profile for moderate level of injection using perturbation theory and Webster effect. The expression of base transit time thus obtained is applicable for all levels of injection. In the next chapter results obtained from the derived equations are plotted.

CHAPTER 4

RESULTS AND DISCUSSION

4.1 INTRODUCTION

In the previous chapter the mathematical equations related to the analytical modeling of base transit time of a non-uniformly doped $Si_{1-y}Ge_y$ base heterojunction bipolar transistor (HBT) have been derived for low and moderate level of injection. Meanwhile necessary computer program has been developed based on the derived equations. Numerical data generated by the program are plotted in this chapter to study the effects of various parameters on the base transit time. The variation of base transit time with different transistor parameters is discussed.

4.2 RESULTS AND DISCUSSION

The results obtained by using the derivations of the previous chapter are analyzed and discussed below.

4.2.1 Distribution of minority carrier within the base

Distribution of injected electron concentration $n(x)$ within the base for three different Ge profiles at a given base doping slope & peak base doping ($N_B(0)$) is shown in Figure 4.1 for (a) low and (b) moderate injection. From Figure 4.1(a)-(b), it is observed that $n(x)$ for triangular Ge profile is lower than that of trapezoidal Ge profile and for box profile, $n(x)$ remains above all other distributions. This is because the transport of electron through the base is assisted by the gradient in Ge profiles [34]. The gradient is the highest for triangular profile, zero for box profile and in-between for trapezoidal profile (referred to Figure 3.1). So for the box Ge profile, electron passes slower through the base to enter the collector and distribution of $n(x)$ remains higher.

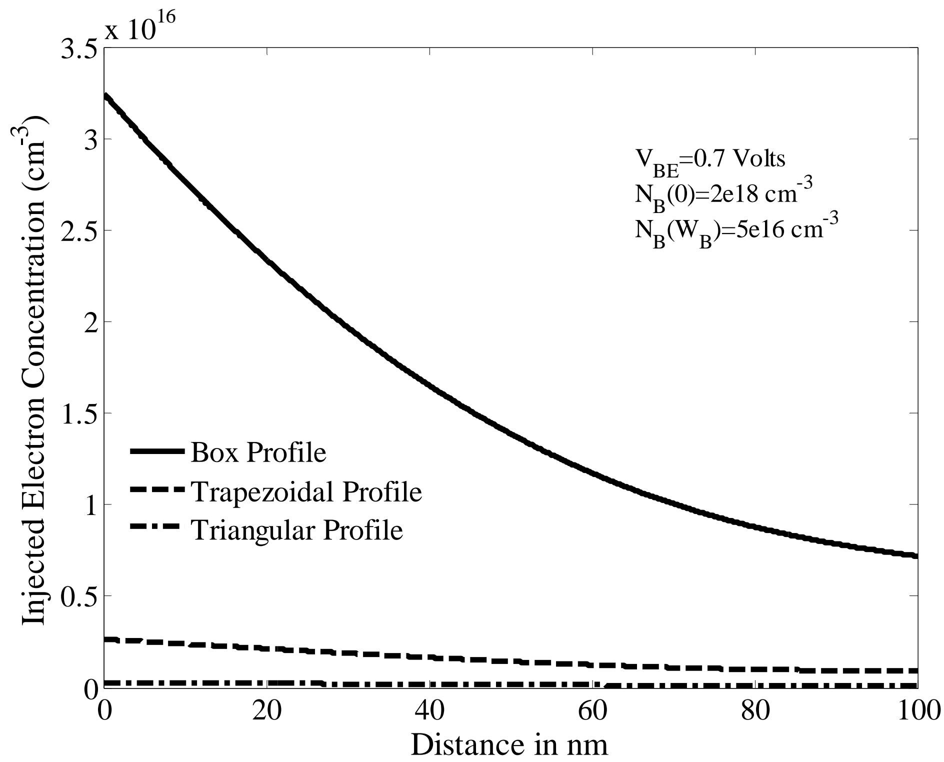

(a)

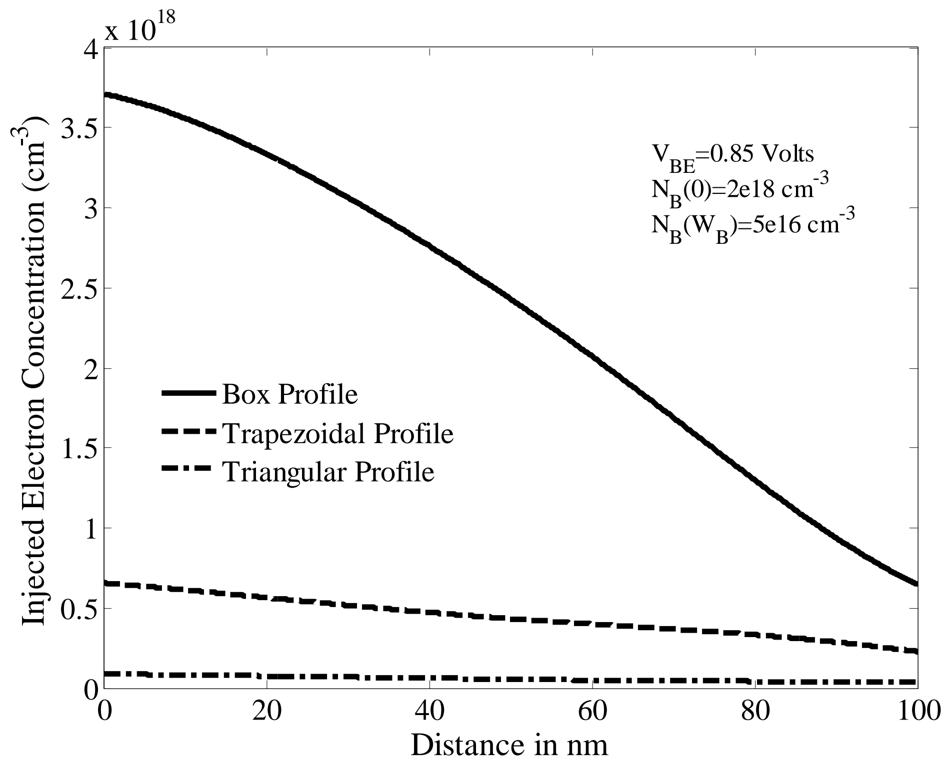

(b)

Figure 4.1: Injected electron distribution within the base for different Ge profiles (Box: y_c=0.2, y_e=0.1999, Trapezoidal: y_c=0.2, y_e=0.1, Triangular: y_c=0.2, y_e=0.01) (a) under low injection (V_{be}=0.7V) (b) under moderate injection (V_{be}=0.85V).

Normalized injected electron distribution ($n(x)/n(0)$) for different base-emitter voltage (V_{be}) (low and moderate injections) at a given $N_B(0)$ and slope of base doping is shown in Figure 4.2(a). It is observed from Figure 4.2(a) that with an increase in V_{be} more electrons are injected from emitter to base. This plot is in good agreement with [69]. In Figure 4.2(b) distribution of ($n(x)/n(0)$) within the base for different $N_B(0)$ at a given V_{be} and slope of base doping are plotted. This figure shows that when $N_B(0)$ increases, more carriers are injected into the base from the emitter which agrees with [70].

The dependence of normalized injected electron distribution on base width (W_B) is shown in Figure 4.3(a). From this plot it is evident that as W_B decreases, ($n(x)/n(0)$) increases. This happens because for shorter base, injected minority carriers get relatively small time to be diffused compared to longer base. So $n(W_B)/n(0)$ for longer base is lower than that of a shorter base. Normalized injected electron distribution also depends on the slope of base doping as appears in Figure 4.3(b). With the increase in the slope of the base doping, $n(\mathrm{x})/n(0)$ decreases more sharply.

The injected electron concentration profiles shown in Figure 4.1(a)-(b), Figure 4.2(a)-(b) and Figure 4.3(a)-(b) are not linear due to the built-in electric field caused by the Gaussian base doping and the gradient in Ge profile. It is also found that the minority carrier has maximum value at the base- emitter junction and minimum value at the collector-base junction. It decreases from its peak value as the distance from the emitter increases. In this work, velocity saturation of electron at the collector-base junction is considered. So at collector-base junction the minority carrier concentrations for low and high levels of injection are not zero.

4.2.2 Variation of minority carrier injection ratio with base-emitter voltage

Variation of minority carrier injection ratio ($n(0)/N_B(0)$) with V_{be} at a given $N_B(0)$, slope of base doping and W_B is shown in Figure 4.4. The figure shows that ($n(0)/N_B(0)$) is an increasing function of V_{be}. From equation (3.24a), it is found that $n(0)$ is exponentially proportional to V_{be}. So, for a given $N_B(0)$, minority carrier injection ratio will also increase exponentially with V_{be} but under moderate injection the exponential slope will

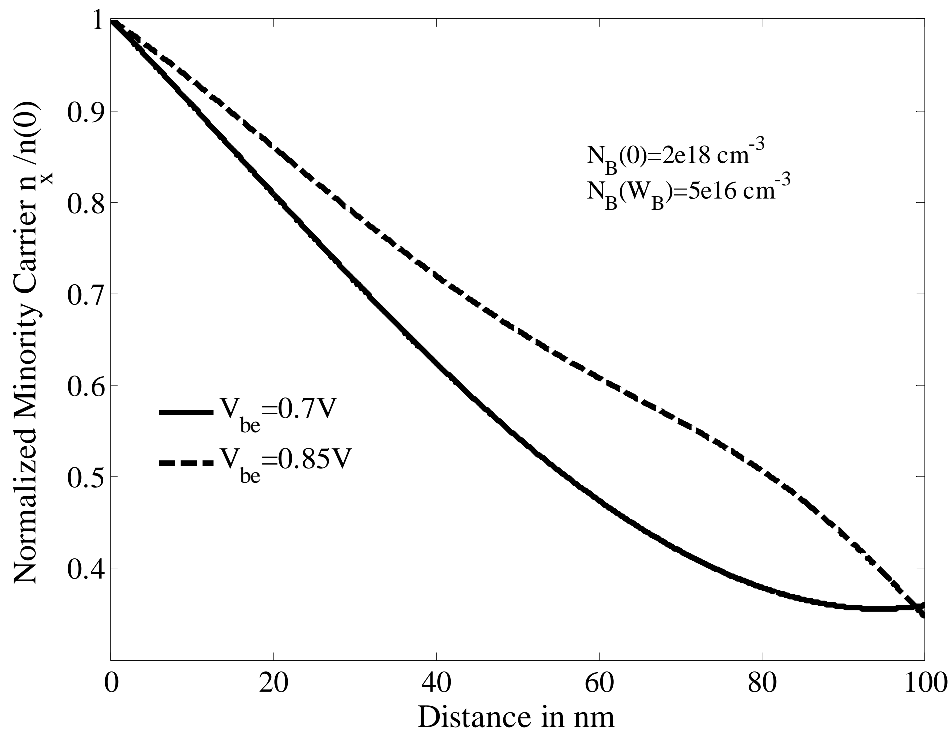

(a)

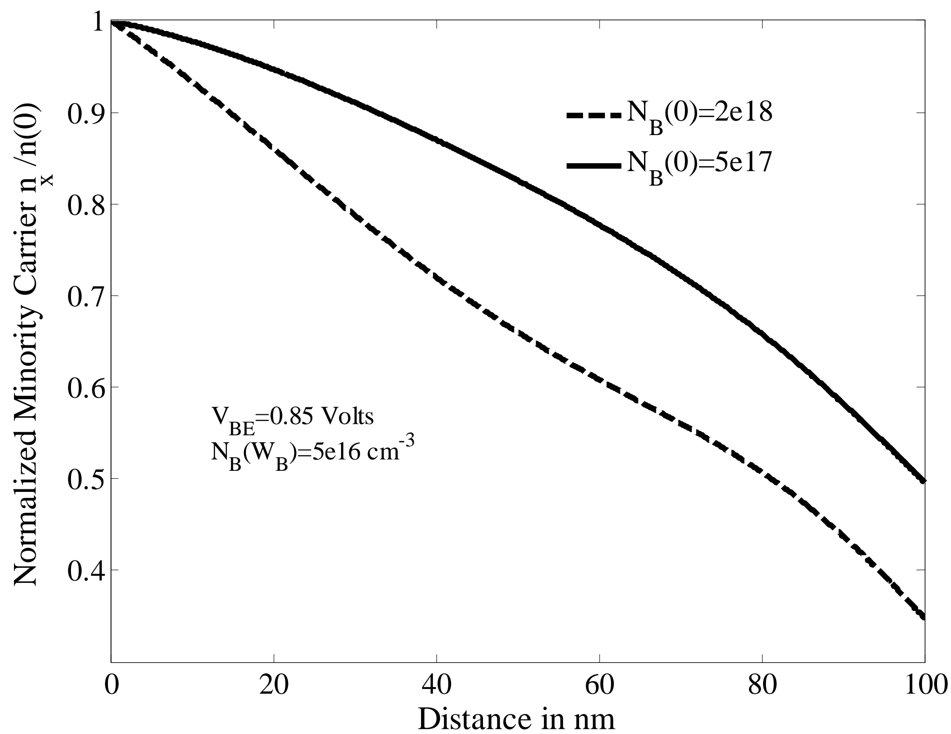

(b)

Figure 4.2: Normalized minority carrier electron distribution within the base (a) for different V_{be} (b) for different $N_B(0)$ with trapezoidal Ge profile (y_c=0.2, y_e=0.1).

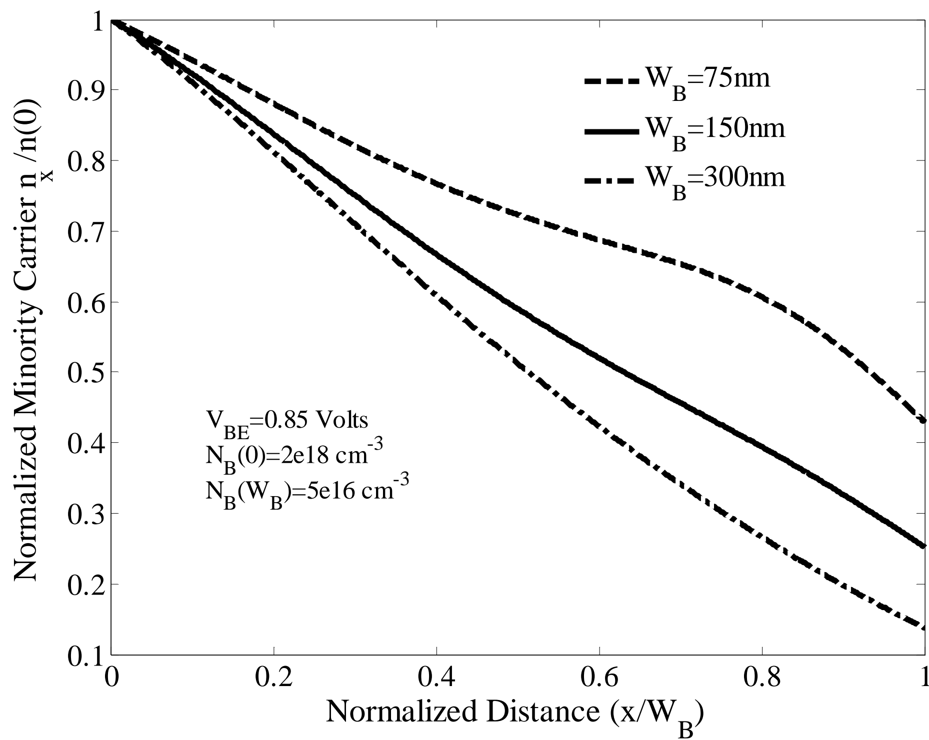

(a)

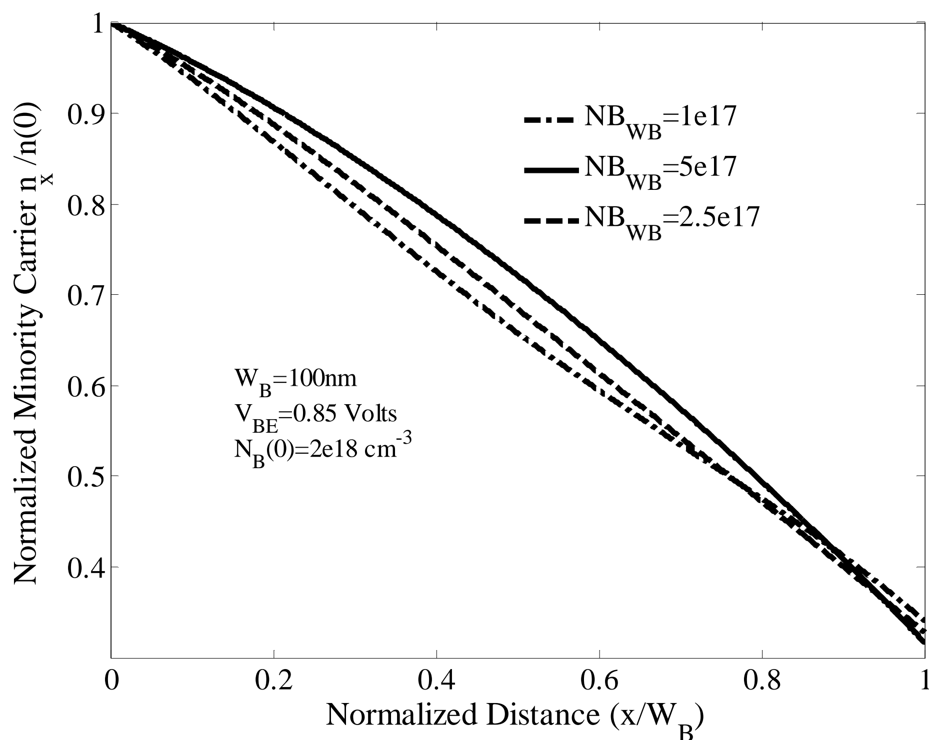

(b)

Figure 4.3: Normalized minority carrier distribution within the base (a) for different base widths (b) for different slopes of base doping with trapezoidal Ge profile (y_c=0.2, y_e=0.1).

decrease due to Kirk effect at a certain high current [18]. For this reason, the low injection part of Figure 4.4 (which is a logarithmic plot) is linear and at the beginning of high injection, its slope starts to fall.

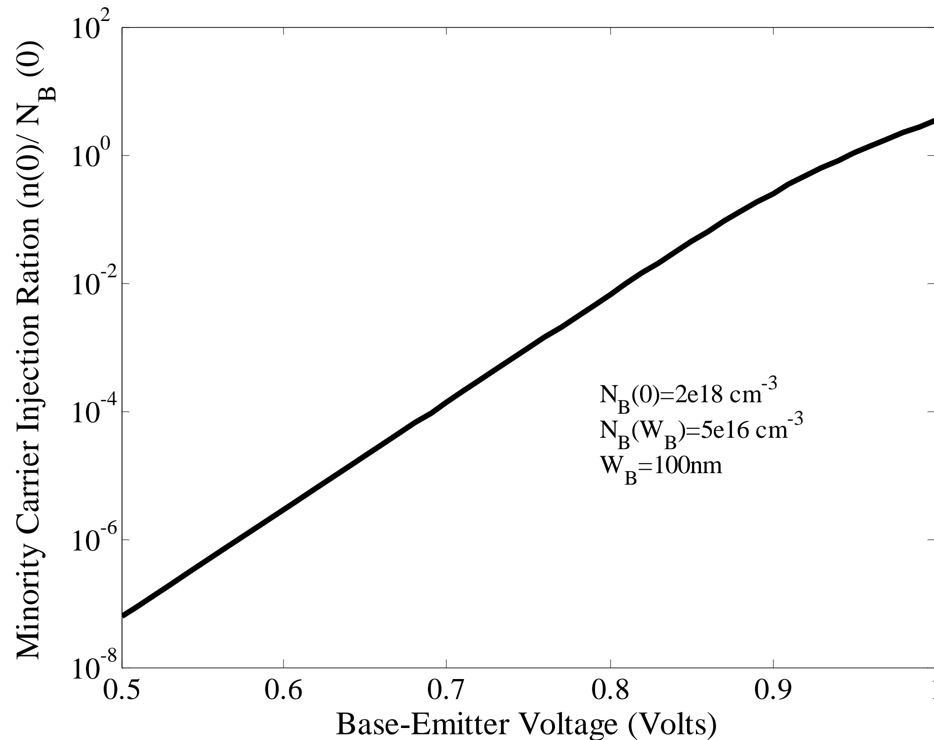

Figure 4.4: Minority carrier injection ratio as a function of base emitter voltage

4.2.3 Variation of collector current density with base-emitter voltage

The variation of collector current density (J_c) with base-emitter voltage (V_{be}) for different shape of Ge profiles is shown in Figure 4.5. For low injection, J_c increases with V_{be} maintaining a constant logarithmic slope; with the increase in V_{be}, the slope of the curves decreases. The plot J_c as a function of V_{be} follows the plot of minority carrier injection ratio ($n(0)/N_B(0)$) with the variation of V_{be} as shown in Figure 4.4. J_c for box shape Ge profile is higher than that of triangular profile and J_c for trapezoidal profile remains in-between. This is expected as the injected electron concentration at the collector-base boundary ($n(W_B)$) is the highest for box shape Ge profile as shown in Figure 4.1 and higher $n(W_B)$ contributes higher J_c as given in (3.29). This finding agrees well with [20].

Figure 4.5 also shows that J_c for the box shape Ge profile declines earlier; later declines that for the trapezoidal profile and J_c for the triangular profile is the last to

decline but all the three curves bend at the same current density. This is due the manifestation of Kirk effect at certain high current density irrespective of Ge profiles and is good agreement with [18].

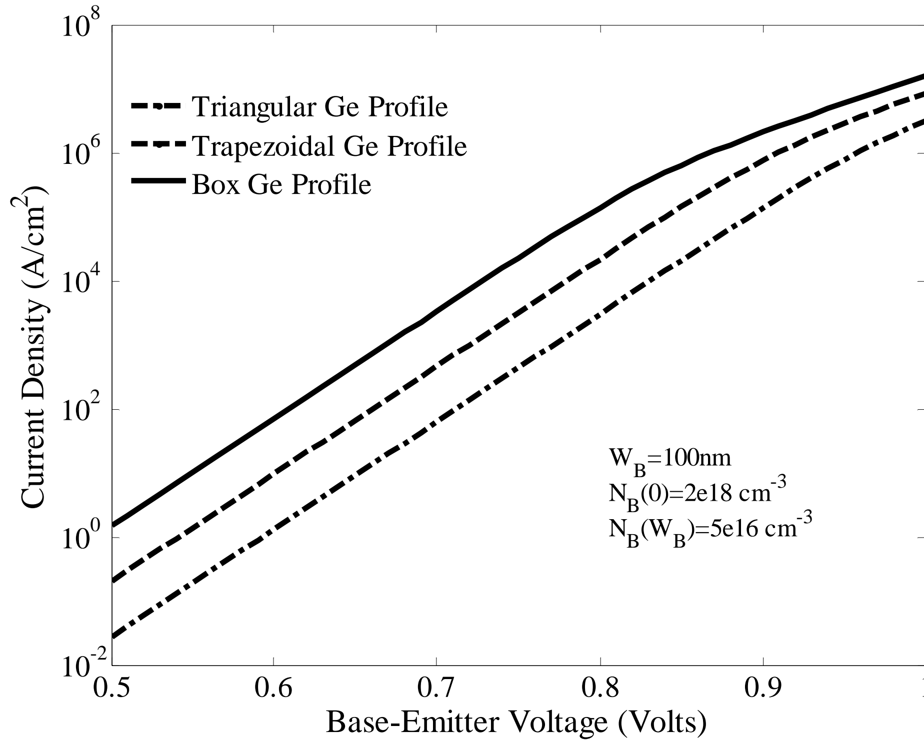

Figure 4.5: Collector current densities for different shape of Ge profiles (Box: y_c=0.2, y_e=0.1999, Trapezoidal: y_c=0.2, y_e=0.1, Triangular: y_c=0.2, y_e=0.01) as a function of base-emitter voltage.

4.2.4 Variation of base transit time with base-emitter voltage

The variations of base transit time (τ_B) with base-emitter voltage (V_{be}) for various Ge profiles are shown in Figure 4.6. It is observed from Figure 4.6 that the base transit time is independent of base-emitter voltage for both low and moderate levels of injection but the value of base transit time is larger for moderate injection region than that of low injection region. This is due to the reduction of aiding field in the Gaussian doped base when the level of injection increases as shown in Figure 4.4-5. Due to this reduction in aiding field, electrons slow down and hence transit time increases. In the intermediate level of injection, base transit time increases as V_{be} increases.

From the Figure 4.6, it also can be observed that box shape Ge profile takes the highest time to pass the electron to the collector, triangular Ge profile takes the lowest

time and the trapezoidal Ge profile takes in-between time. This is related to the gradient of Ge profiles as discussed in article 4.2.1. This result is also validated by [20] which shows that transit through the base is a minimum when the triangular Ge profile is chosen.

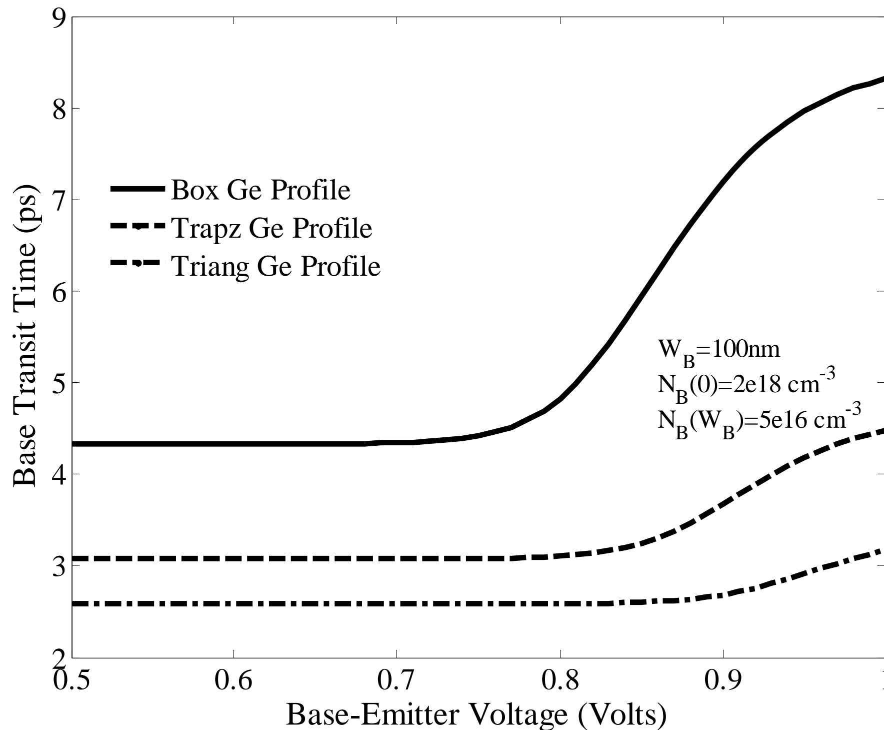

Figure 4.6: Base transit time as a function of base-emitter voltage for different shape of Ge profiles (Box: y_c=0.2, y_e=0.1999, Trapezoidal: y_c=0.2, y_e=0.1, Triangular: y_c=0.2, y_e=0.01).

4.2.5 Variation of base transit time with minority carrier injection ratio

As discussed earlier in article 4.2.2, minority carrier injection ratio is an increasing function of base-emitter voltage. So, the variation of the base transit time with the minority carrier injection ratio has the same pattern as the base transit time varies with base-emitter voltage (Figure 4.6). The variation of base transit time with the minority carrier injection ratio for box shape Ge profile is revealed in Figure 4.7. With the increase of minority carrier injection ratio, the aiding field reduces, electron slows down and the base transit time increases.

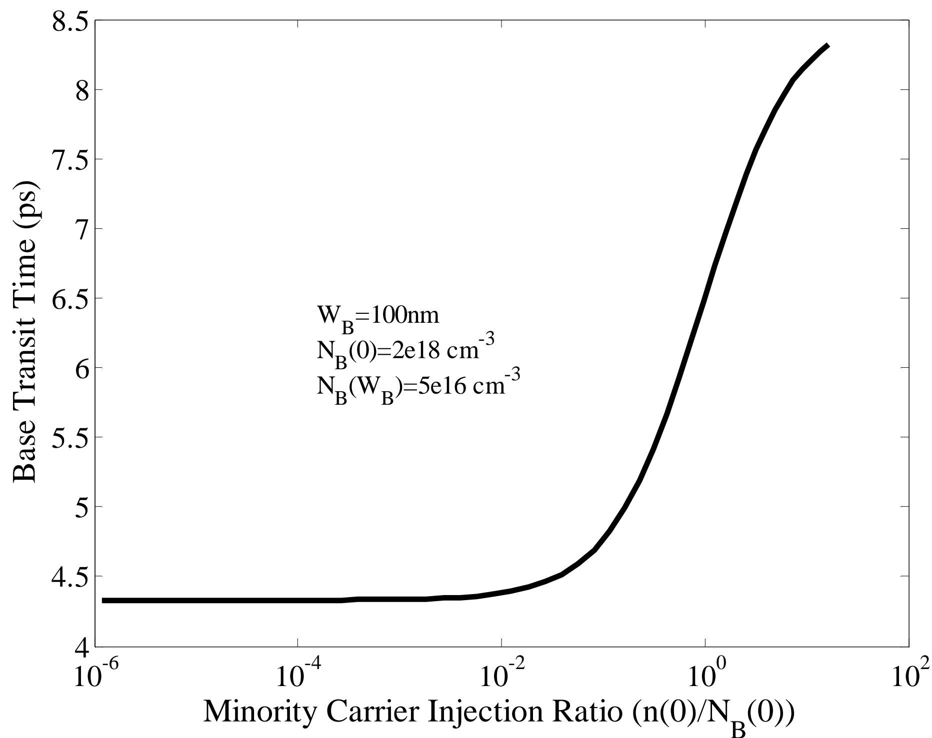

Figure 4.7: Base transit time as a function of minority carrier injection ratio for box shape Ge profile (y_c=0.2, y_e=0.1999). Doping dependent mobility is considered.

4.2.6 Dependence of base transit time upon base width

The dependence of base transit time (τ_B) upon base width (W_B) for different $N_B(0)$ at a given base profile is shown in Figure 4.8(a)-(b). From these figures it is clear that τ_B is an increasing function of W_B as was found in the mathematical analysis. With the increase in W_B, the stored base charge increases and $n(W_B)$ decreases (shown in Figure 4.3(a)); this results in a reduction in electron current density as defined by equation (3.29), eventually the base transit time experiences two fold increase as per (3.32). For constant W_B, slope of base doping and $N_B(0)$, τ_B is smaller for low injection (dashed line) than that of moderate injection (solid line).

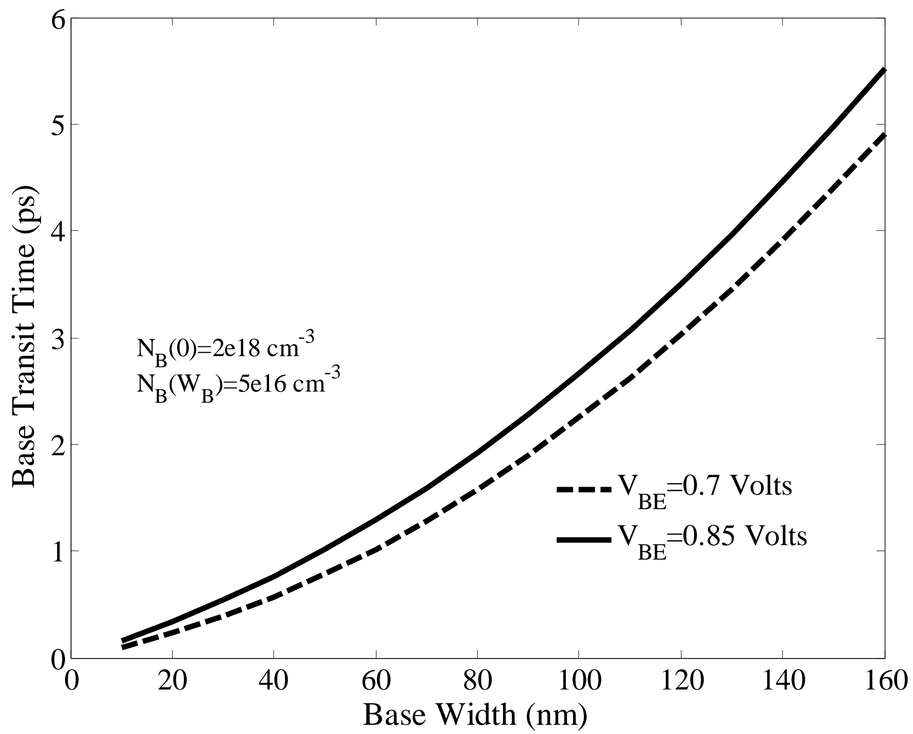

(a)

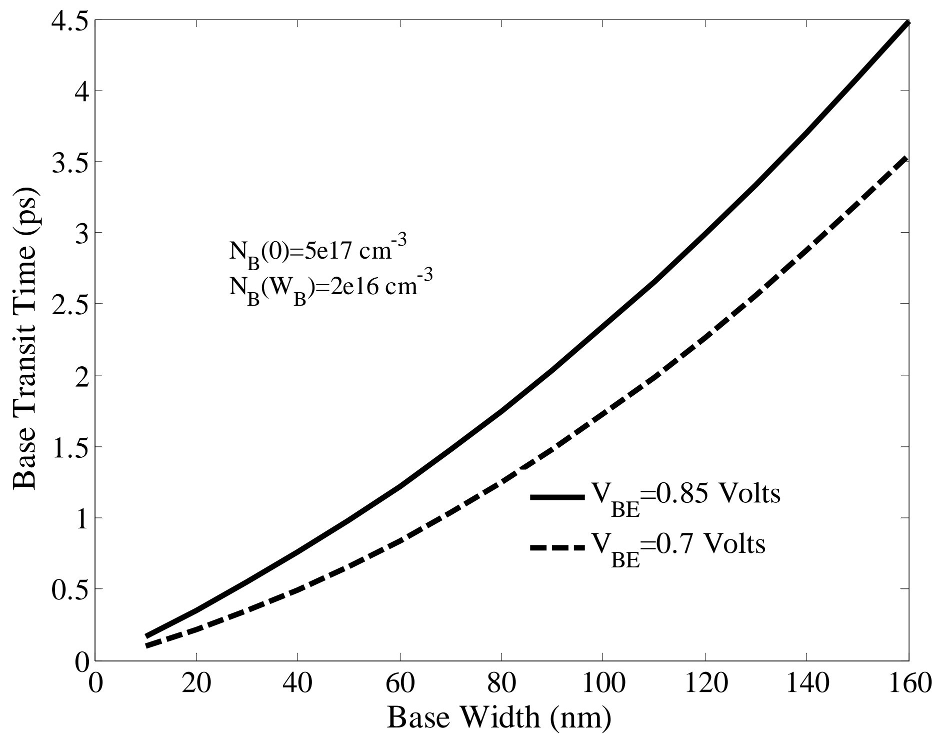

(b)

Figure 4.8: Base transit time as function of base width (a) for heavily doped base (b) for a comparatively lightly doped base HBT with trapezoidal Ge profile (y_c=0.2, y_e=0.1).

4.2.7 Dependence of base transit time upon peak base doping concentration

The dependence of base transit time upon peak base doping concentrations is shown in Figure 4.9. From the figure it is found that the base transit time increases with peak base concentration. Equation (3.12a) shows that $D_n(\mu_n)$ decreases with $N_B(0)$. For low level of injection $E(x)$ is given by eqn. (3.17b). It shows that $E(x)$ is independent of $N_B(0)$. Due to the decrease of $D_n(\mu_n)$ the stored base charge increases resulting in an increase of τ_B. For high level of injection $E(x)$ reduces in amplitude. The decrease in both the aiding electric field and the mobility contribute to the increase of τ_B.

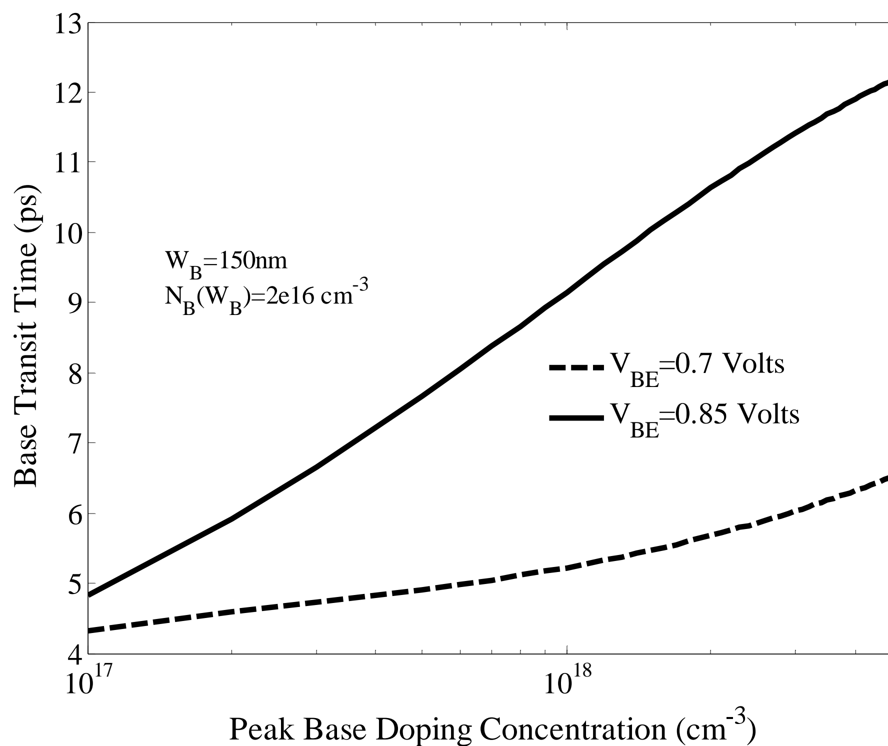

Figure 4.9: Base transit time as a function of peak base doping concentration with a box shape Ge profile (y_c=0.2, y_e=0.1999) for moderate and low level of injection.

4.2.8 Dependence of base transit time upon field dependent mobility

One of the main objectives of this research work is to obtain base transit time of an Gaussian doped base $Si_{1-y}Ge_y$ HBT considering electric field dependence of carrier mobility in excess to doping dependent mobility. The effect of electric field dependence of mobility on base transit time was investigated and the result is shown in Figure 4.10. The transit time is found to be higher if the field dependence of mobility is considered.

This is because minority carrier mobility is inversely related to the absolute value of electric field (3.14a). With the increase in electric field, minority carrier mobility in the base region decreases. So, with the increase in electric field, it decreases the minority carrier transportation through the base region and hence contributes to the increase in base transit time.

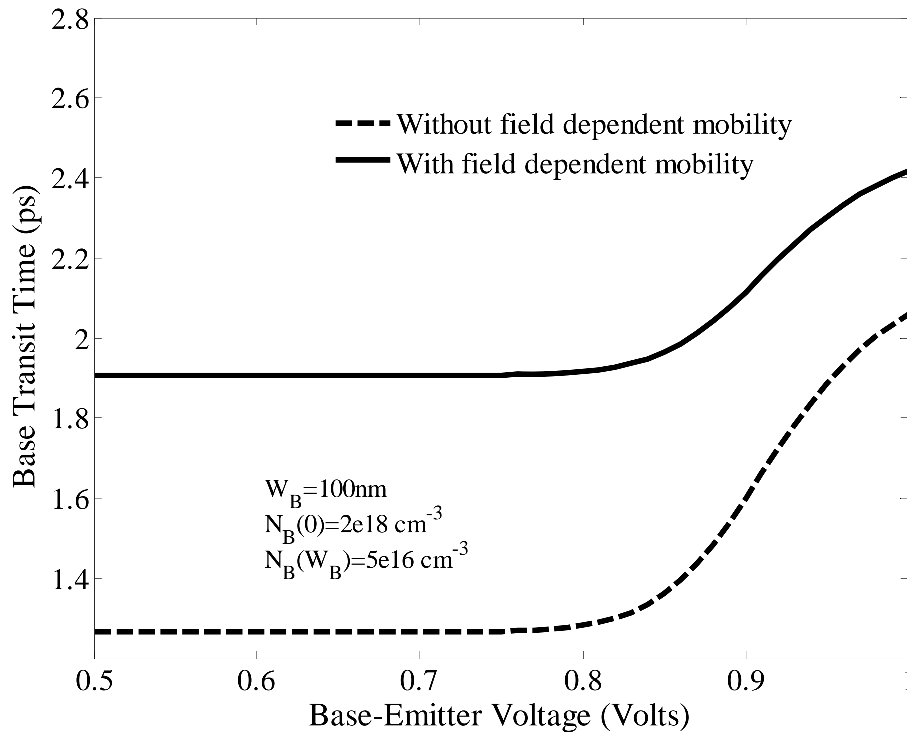

Figure 4.10: Base transit time as a function of base-emitter voltage with and without field dependent electron mobility. A triangular Ge profile (y_c=0.2, y_e=0.01) is considered.

4.2.9 Dependence of base transit time upon slope of base doping

Effect of change in the slope of base doping on base transit time (τ_B) is also studied and the results are shown in Figure 4.11. From the Figure 4.11, it is found that the base transit time is a decreasing function of the slope of base doping for both low (dashed line) and moderate (solid line) level of injection. This is because with the increase in slope of base doping, the injected electron concentration profile becomes steeper (Figure 4.3(b)) which eventually reduces the stored base charges (area under $n(x)$ profile) and the base transit time decreases.

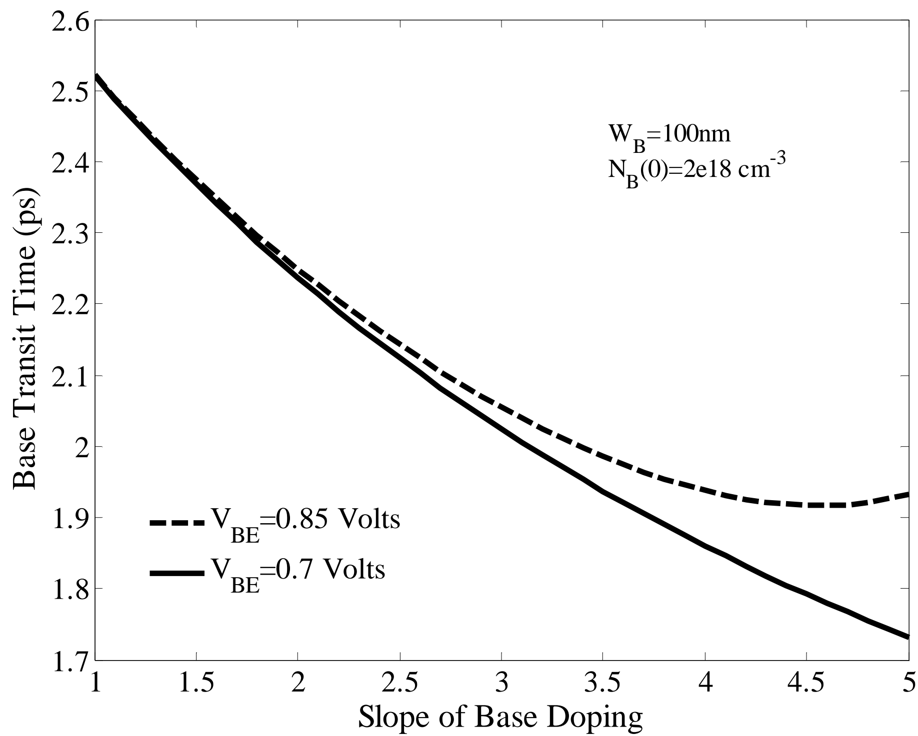

Figure 4.11: Base transit time as a function of slope of base doping with a triangular shape Ge profile (y_c=0.2, y_e=0.01) for moderate and low level of injection.

4.2.10 Dependence of base transit time upon peak Ge fraction

The base transit time of a $Si_{1-y}Ge_y$ base heterojunction bipolar transistor also depends on peak Ge fraction (y_C). The variation of base transit time with y_C is shown in Figure 4.12. It is observed from the figure that both for uniform ($N_B(W_B)$=1e18) and Gaussian ($N_B(W_B)$=5e16) base doping with triangular Ge profile in the base, the transit time decreases as the values of the peak Ge fraction increases. This happens because increasing y_C (keeping y_E=0), increases both the amount of Ge grading (η_{Ge}) and the Ge dose (y_D). This gives rise to a drift field which consequently decreases the base transit time of the HBT.

Similar trends are found with exponentially doped base as reported in [72]. In this comparison, doping dependent mobility is considered.

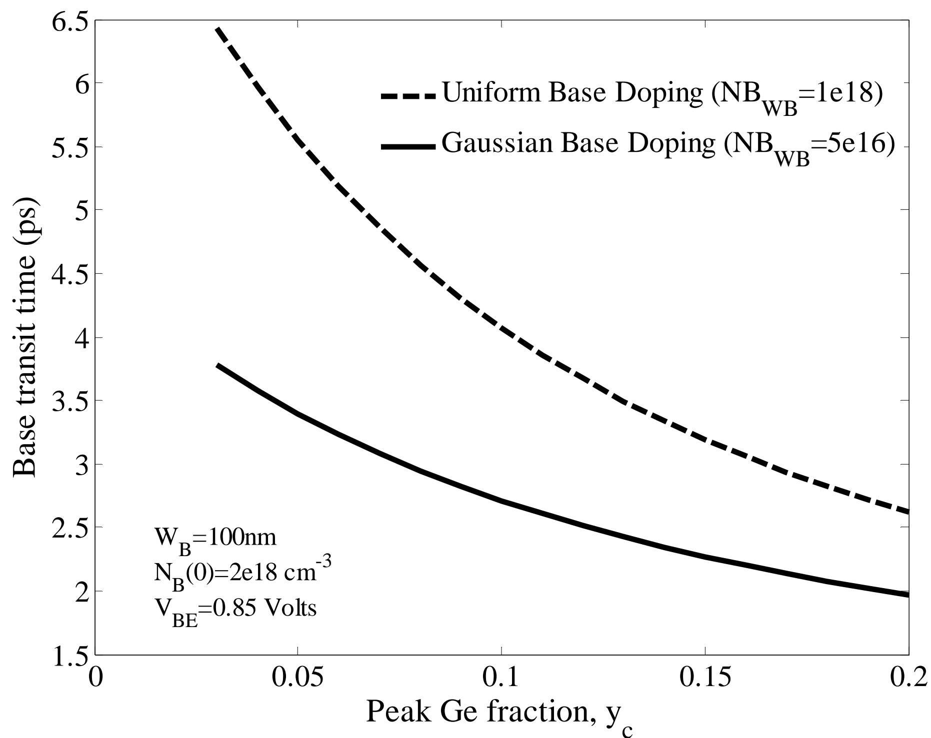

Figure 4.12: Base transit time as a function of peak Ge % (y_C) for triangular Ge profile with uniform and Gaussian doped base.

4.2.11 Dependence of base transit time upon collector current density

The variation of base transit time (τ_B) with collector current density for different Ge profiles is shown in Figure 4.13. From the Figure 4.13, it is understandable that base transit time is independent of collector current density for both low and moderate level of injection. But the value of base transit time is larger for moderate injection region than the base transit time for low injection region. This is due to the reduction of aiding electric field in the Gaussian doped base when the level of injection increases. Due to this effect, electrons slow down and transit time increases. In the intermediate level of injection, base transit time increases as J_c increases. From the Figure 4.13, it is also perceptible that box shape Ge profile takes higher transit time than triangular Ge profile to pass the electron to the collector and the trapezoidal Ge profile takes in-between time. This happens due to the difference in gradients of Ge profiles. It is noticeable that Figure 4.13 follows Figure 4.6 (τ_B vs. V_{be}) as collector current is a logarithmic function of V_{be} (Figure 4.5).

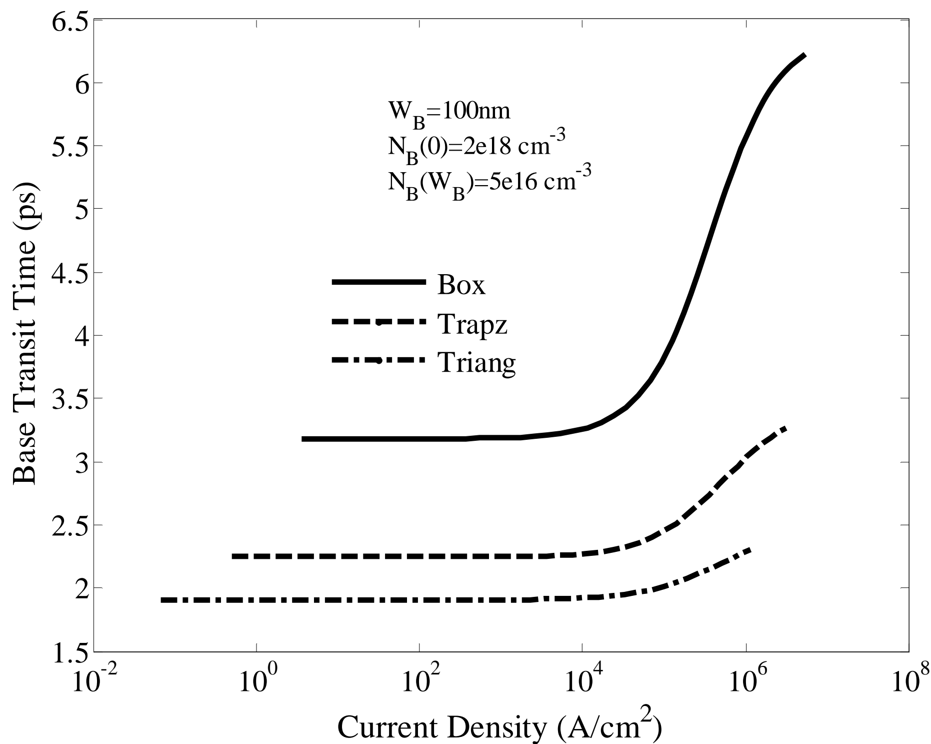

Figure 4.13: Base transit time as a function of collector current density for different shape of Ge profiles (Box: y_c=0.2, y_e=0.1999, Trapezoidal: y_c=0.2, y_e=0.1, Triangular: y_c=0.2, y_e=0.01).

4.2.12 Comparison of base transit time with HBT

Variation of base transit time with Ge concentration at the collector edge is plotted in Figure 4.14 and is compared with [26] to prove the validity of the proposed model. The calculated result with present model shows similar trends for transit time with peak Ge concentration as compared with the published results. As the published results adopted different technique and parameter values to evaluate base transit time, it was difficult to match the results with choosing suitable parameter values. This is why there is some deviation within the calculated and published values.

4.2.13 Comparison of collector current with BJT

Variation of collector current with base to emitter voltage is plotted in Figure 4.15(a) and is compared with [34] to prove the validity of the proposed model. It demonstrates that collector current for SiGe HBT is higher than Si BJT and consequently produces smaller transit times for HBT than BJT. Figure 4.15(b) demonstrates the difference between calculated currents for HBT and BJT. The solid line represents results found with the proposed model and dashed line is for those found from [34].

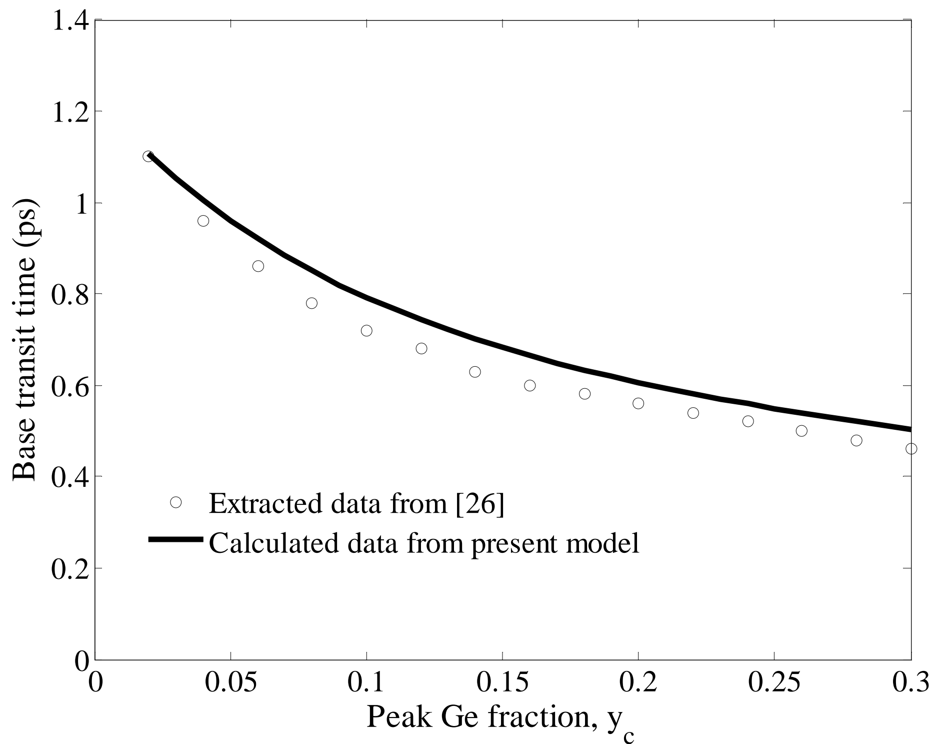

Figure 4.14: Comparison of base transit time with Ge concentration at the collector edge [26].

4.2.14 Comparison of transit time and current density with BJT

Variation of collector current density with base to emitter voltage is plotted in Figure 4.16(a) and is compared with [73]. It demonstrates that collector current density for Si BJT with Gaussian doping profile is higher than that with uniform doping. Figure 4.16(b) demonstrates variation of base transit time with minority carrier injection ratio ($n(0)/N_B(0)$). The comparison shows close resemblance for the Gaussian variation rather than uniform doping.

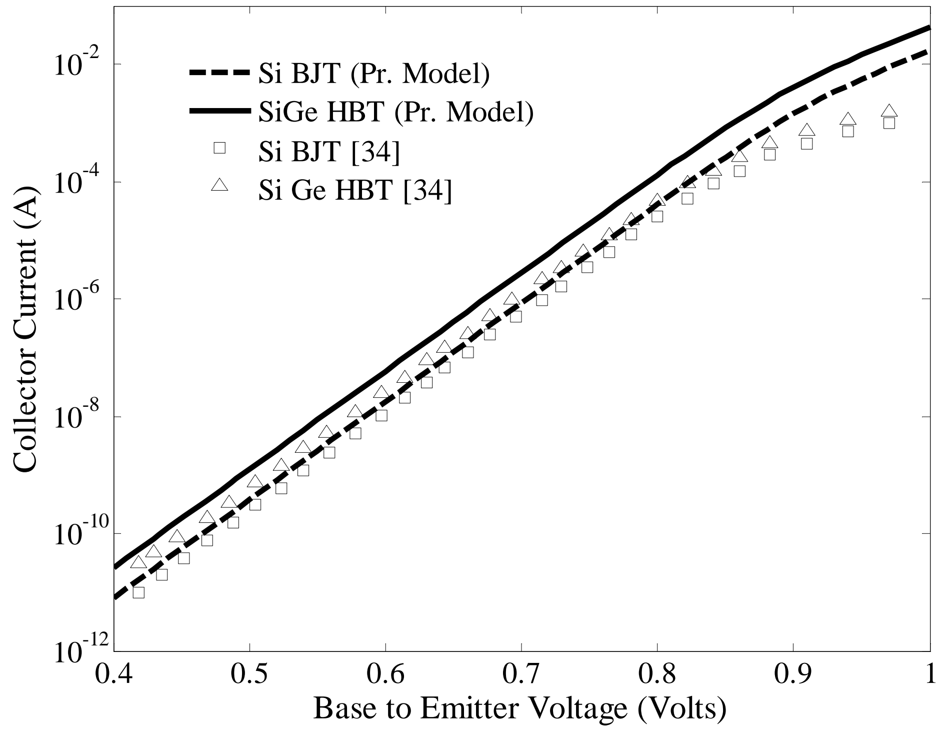

(a)

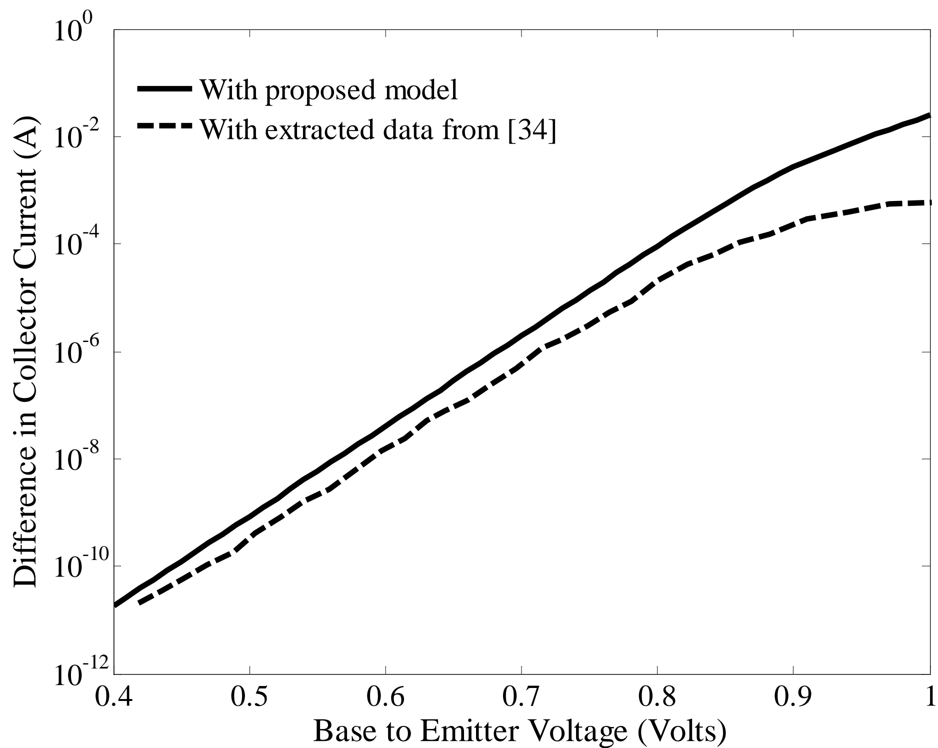

(b)

Figure 4.15: a) Collector current as a function of base-emitter voltage and b) Difference in collector current as a function of base-emitter voltage for Si BJT and SiGe HBT. The calculated values are compared with Gummel Characteristics reproduced from [34].

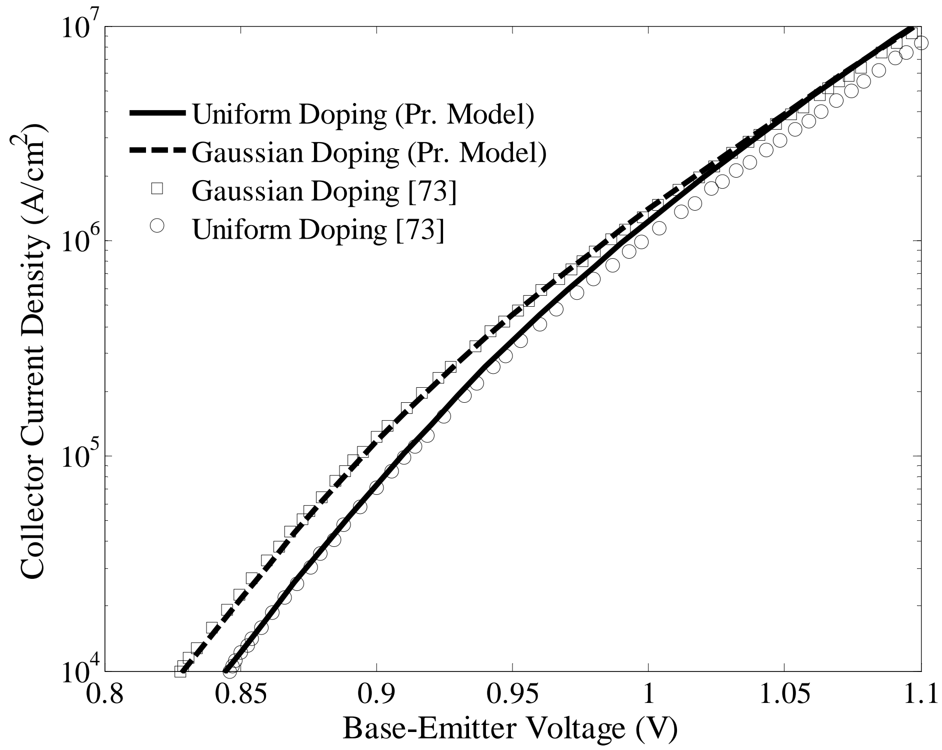

(a)

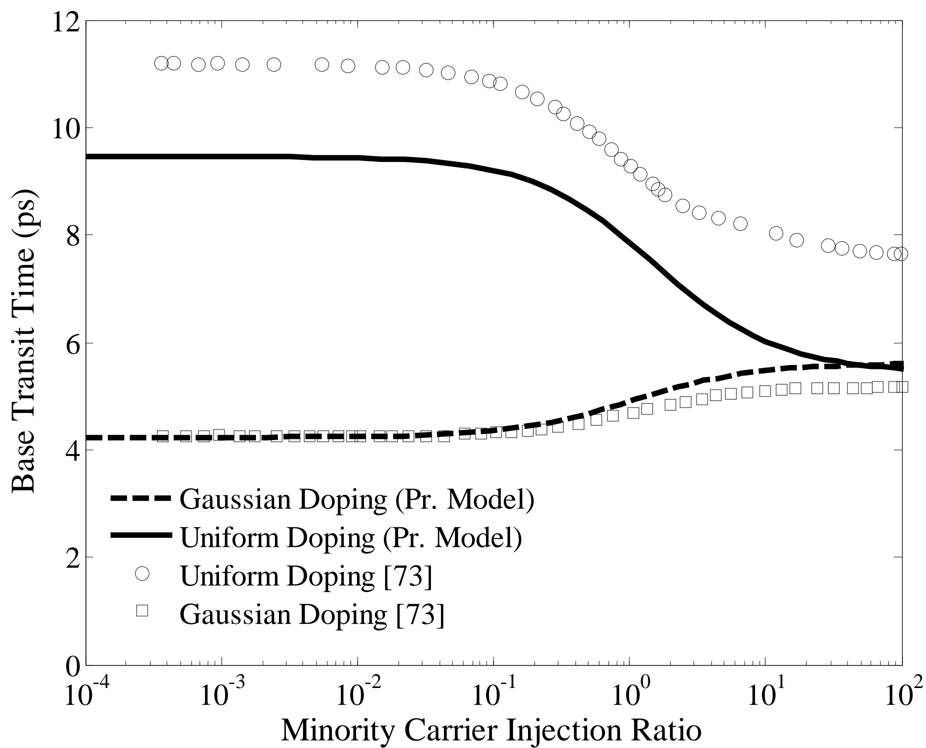

(b)

Figure 4.16: a) Collector current density as a function of base-emitter voltage and b) Base transit time as a function of minority carrier injection ratio for Si BJT. The calculated values are compared with P. Ma results [73].

4.3 CONCLUSION

The analytical expression obtained in chapter two is used to determine the dependence of base transit time on different parameters of HBT. The results show that base transit time increases with base-emitter voltage, minority carrier injection ratio, base width, peak base doping concentration, saturation velocity and field dependent mobility. On the other hand base transit time decreases with gradient in Ge profiles.

CHAPTER 5

CONCLUSION AND SUGGESTIONS

5.1 CONCLUSION

The base transit time of a nonuniformly doped base (Gaussian doping) $Si_{1-y}Ge_y$ HBT with different type of Ge profiles for all levels of injection has been studied to develop an analytical model by first obtaining solution of minority carrier injected into the base under low level of injection. But for moderate level of injection, differential equation governing the minority carrier concentration is not analytically tractable. For this, the low level analytical solution is extended for moderate level of injection using perturbation theory and Webster effect and the obtained model is applicable for all levels (both low and moderate) of injection. In doing this, electric field and doping dependent mobility, bandgap narrowing effect due to heavy doping, presence of Ge and change in the density of states, velocity saturation at collector-base junction (modified to address the presence of Ge) etc. have been considered to study the injected minority carrier, collector current density, stored base charge and hence the base transit time. The analysis shows that the base transit time increases with base-emitter voltage, minority carrier injection ratio, base width and peak base doping concentration & if finite carrier velocity at the collector edge and dependence of mobility on electric field are considered while it decrease with slope of doping and gradient in Ge profiles. It is found that the transit time decreases with the change in Ge profile from box to triangle. The analytical expressions derived in the present model can be a useful tool in device design and optimization.

5.2 SUGGESTIONS FOR FUTURE WORK

In this work, three different Ge profiles (box type, triangular or trapezoidal shape as shown in Fig. 3.1) were considered where peak of the Ge mole fraction (y_C) was located on the collector end of the base. Another trapezoidal Ge profile with variable peak position is reported in literature where base transit time is obtained numerically. In future, such a dual slope Ge profile may be considered for analytical treatment.

An Gaussian doped base profile was considered for this work. In future other non-uniform base doping profiles like retrograde or epitaxial base doping can be considered for the calculation of base transit time of a SiGe HBT.

A model for all level (low and moderate) of injection of a SiGe base HBT has been developed but at strong high level of injection the phenomenon known as Kirk effect will occur which is not addressed here. When the Kirk effect occurs the base transit time will become large and will increase with J_c. In future, an expression for base transit time considering Kirk effect may be carried out.

Like the improvement in base transit time of HBT in comparison with BJT, improvement also are predicted for current gain, Early voltage (hence out put resistance), base resistance and cutoff frequency (hence maximum oscillation frequency). These can be investigated in future.

The HBT considered here was a SiGe based heterojunction bipolar transistor. Attempt should be taken to investigate the base transit time using our model for InP, AlGaAs etc based HBT.

REFERENCES

[1] Hochheiser S., "The Transistor and Portable Electronics," IEEE Global History Network, 2008.

[2] Arns R. G., "The other transistor: early history of the metal-oxide-semiconductor field-effect transistor," *Engineering Science and Education Journal,* vol. 7, pp. 233–240, October 1998.

[3] Heywang W. and Zaininger K. H., *Silicon: The semiconductor material, evolution and future of a technology*, Springer, 2004.

[4] Moll J. L. and Ross I. M., "The dependence of transistor parameters on the distribution of base layer resistivity," *Proc. IRE,* vol. 44, pp. 72-78, Jan 1956.

[5] Biesen J. J. H. V. D., "A simple regional analysis of transit times in bipolar transistors," *Solid-State Electronics,* vol. 29, pp. 529–534, 1986.

[6] Suzuki K. and Nakayama N., "Base transit time of shallow-base bipolar transistor considering velocity saturation at base-collector junction," *IEEE Trans. on Electron Devices,* vol. 39, pp. 623-628, 1992.

[7] Jahan M. M. and Anwar A. F. M., "An analytical expression for base transit time in an exponentially doped base bipolar transistor," *Solid-State Electronics,* vol. 39, pp. 133-136, January 1996.

[8] Rinaldi N., "Analytical relations for the base transit time and collector current in BJTs and HBTs," *Solid-State Electronics,* vol. 41, pp. 1153-1158, 1997.

[9] Patri V. S. and Kumar M. J., "Profile Design Considerations for minimizing base transit time in SiGe HBT's," *IEEE Trans. on Electron Devices,* vol. 45, pp. 1725-1731, Aug 1998.

[10] Kwok K. H., "Analytical expressions of base transit time for SiGe HBTs with retrograde base profiles," *Solid-State Electronics,* vol. 43, pp. 275-283, 1999.

[11] Hassan M. M. S. and Khandoker A. H., "New expression for base transit time in a bipolar junction transistor for all level of injection," *Microelectronics Reliability,* vol. 41, pp. 137-140, 2001.

[12] Li G., Neugroschel A., Sah C. T., Hemmenway D., Rivoli T., and Maddux J., "Analysis of bipolar junction transistors with Gaussian base-dopant impurity-concentration profile," *IEEE Trans. on Electron Devices,* vol. 48, pp. 2945-2947, 2001.

[13] Khan M., Hassan M., and Rahman T., "Empirical Expression for Base Transit Time in Bipolar Transistors," *International Journal of Electronics,* vol. 92, pp. 215-229, April 2005.

[14] Mohammedy F. M. and Hassan M. M. S., "A distributed transmission line model for the base transit time of a nonuniformly doped BJT," in *Second International Conference on Electrical and Computer Engineering, ICECE 2002* Dhaka, Bangladesh, 2002.

[15] Abedin M. A. and Hassan M. M. S., "Base transit time model of a bipolar junction transistor considering Kirk effect," *Journal of The Institution of Engineers, Singapore,* vol. 45, pp. 48-61, 2005.

[16] Rahman T., Khan M. Z. R., and Hassan M., "Base Transit Time of a Bipolar Transistor with Gaussian Base Doping Profile," *IEB Journal of Electrical Engineering,* vol. EE 31, pp. 6 - 9, DEC 2004.

[17] Nomani M. W. K. and Hassan M. M. S., "A new technique for determining base transit time of a BJT," in *4th International Conference on Electrical and Computer Engineering, ICECE 2006* Dhaka, Bangladesh, 2006, pp. 56-59.

[18] Kwok K. H. and Selvakumar C. R., "Profile design considerations for minimizing base transit time in SiGe HBTs for all levels of Injection before onset of Kirk effect," *IEEE Trans. on Electron Devices,* vol. 48, pp. 1540-1549, 2001.

[19] Chang S. T., Liu C. W., and Lu S. C., "Base transit time of graded-base Si/SiGe HBTs considering recombination lifetime and velocity saturation," *Solid-State Electronics,* vol. 48, pp. 207–215, 2004.

[20] Das M. K., Das N. R., and Basu P. K., "Effect of Ge content and profile in the SiGe base on the performance of a SiGe/Si HBT," *Microwave and Optical Technology Letters,* vol. 47, pp. 247-254, Nov 2005.

[21] Basu S., "Analytical modelling of base transit time of SiGe HBTs including effect of temperature," *International Semiconductor Conference, CAS'08,* vol. 2, pp. 339-342, Oct 2008.

[22] Suzuki K., "Analytical base transit time model for high-injection regions," *Solid-State Electronics,* vol. 37, pp. 487-493, 1994.

[23] Ma P., Zhang S. L., and Stling M. O., "A new set of initial conditions for fast and accurate calculation of base transit time and collector current density in bipolar transistors," *Solid-State Electronics,* vol. 42, pp. 2023-2026, 1998.

[24] Hassan M. M. S. and Nomani M. W. K., "Base transit time model considering field dependent mobility for BJTs operating at high-level injection," *IEEE Trans. on Electron Devices,* vol. 53, pp. 2532-2539, Oct 2006.

[25] Arafat Yeasir, Khan M. Z. R. and Hassan M. M. S., "Base Transit Time of a Heterojunction Bipolar Transistor with Exponentially Doped Base," Journal of Electrical Engineering, The Institution of Engineers, Bangladesh, Vol. EE 36, No. I, pp. 52-57, June 2009

[26] Zareba A. and Jakubowski Z., "Optimization of selected parameters of SiGe HBT transistors," *Journal of Telecommunications and Information Technology,* 3-4, 2000.

[27] Snowden C. M. and Snowden E., *Introduction to Semiconductor Device Modelling*, 1 ed.: World Scientific Publishing Co, Singapore, 1998.

[28] Sze S. M. and Ng K. K., *Physics of Semiconductor Devices*, 3rd ed. New Jersey: Jown Wiley & Sons, 2007.

[29] Levy R. A., *Microelectronic Materials and Processes*: Kluwer Academic Publisher, 1989.

[30] Streetman B. G., *Solid State Electronic Devices*, 4th ed.: Prentice Hall, 1995.

[31] Grens C. M., Cheng P., and Cressler J. D., "An Investigation of the Large-Signal RF Safe-Operating-Area on Aggressively-Biased Cascode SiGe HBTs for Power Amplifier Applications," 2009.

[32] Asbeck P., *Handbook of Thin Film Devices* vol. 1: Academic Press, 2000.

[33] "The Nobel Prize in Physics," URL http://nobelprize.org/nobel_prizes/2000.

[34] Cressler J. D. and Niu G., *Silicon-Germanium Heterojunction Bipolar Transistors*. Norwood, MA: Artech House, 2003.

[35] Jain S. C., *Germanium-Silicon Strained Layers and Heterostructures*: Academic Press, Inc. USA, 1994.

[36] Harame D. L., Ahlgren D. C., Coolbaugh D. D., Dunn J. S., Freeman G. G., Gillis J. D., Groves R. A., Hendersen G. N., Johnson R. A., Joseph A. J., Subbanna S., Victor A. M., Watson K. M., Webtser C. S., and Zampardi P. J., "Current status

and future trends of SiGe BiCMOS Technology," *IEEE Trans. on Electron Devices,* vol. 48, p. 2575−2593, Nov 2001.

[37] Zhang G., Cressler J. D., Niu G., and Pinto A., "A comparison of npn and pnp profile design tradeoffs for complementary SiGe HBT technology," *Solid-State Electronics,* vol. 44, p. 1949−1954, 2000.

[38] Lombardo S., Raineri V., Via F. L., Iacona F., Campisano S. U., Pinto A., and Ward P., "Ge-ion implantation in silicon for the fabrication of silicon/SiGe heterojunction transistors," *Material Chemistry and Physics,* vol. 46, p. 156−160, 1996.

[39] Hamel J. S., Tang Y. T., and Osman K., "Technological requirements for a lateral SiGe HBT technology including theoretical performance predictions relative to vertical SiGe HBTs," *IEEE Trans. on Electron Devices,* vol. 49, p. 449−456, March 2002.

[40] Ahlgren D. C., Freeman G., Subbanna S., Groves R., Greenberg D., Malinowski J., Nguyen-Ngoc D., Jeng S. J., Stein K., Schonenberg K., Kiesling D., Martin B., Wu S., Harame D. L., and Meyerson B., "A SiGe HBT BiCMOS technology for mixed-signal RF applications," *Proceedings of the Bipolar/BiCMOS Circuits and Technology Meeting,* pp. 195-197, September 1997.

[41] Joseph A., Coolbaugh D., Zierak M., Wuthrich R., Geiss P., He Z., Liu X., Orner B., Johnson J., Freeman G., Ahlgren D., Jagannathan B., Lanzerotti L., Ramachandran V., Malinowski J., Chen H., Chu J., Gray P., Johnson R., Dunn J., Subbanna S., Schonenberg K., Harame D., Groves R., Watson K., Jadus D., Meghelli M. and Rylyakov A., "A 0.18um BiCMOS technology featuring 120/100 GHz (fT/fmax) and ASIC-compatible CMOS using copper interconnect," *Proceedings of the Bipolar/BiCMOS Circuits Circuit Tech. Meeting, Minneapolis,* pp. 143-146, October 2001.

[42] Heinemann B., Rucker H., Barth R., Bauer J., Bolze D., Bugiel, Drews J., Ehwald K.E., Grabolla T., Haak U., Hoppner W., Knoll D., Kruger D., Kuck B., Kurps R., Marschmeyer M., Richter H. H., Schley P., Schmidt D., Scholz R., Tillack B., Winkler W., Wolnsky D., Wulf H.-E., Yamamoto Y., and Zaumseil P., "Novel collector design for high-speed SiGe:C HBTs," *IEEE International Electron Device Meeting Technical Digest,* pp. 775-778, December 2002.

[43] Heinemann B., Barth R., Bolze D., Drews J., Formanek P., Grabolla T., Haak U., Hoppner W., Knoll D., Kopke K., Kuck B., Kurps R., Marschmeyer S., Richter H. H., H. Rucker, Schley P., Schmidt D., Winkler W., Wolansky D., Wulf H.-E., and Yamamoto Y., "A low-parasitic collector construction for high-speed SiGe:C HBTs," *IEEE International Electron Device Meeting Technical Digest,* pp. 251-254, December 2004.

[44] Heinemann B., Barth R., Bolze D., Drews J., Formanek P., Fursenko O., Glante M., Glowatzki K., Gregor A., Haak U., Hoppner W., Knoll D., Kurps R., Marschmeyer S., Orlowski S., Rucker H., Schley P., Schmidt D., Scholz R., Winkler W., and Yamamoto Y., "A complementary BiCMOS technology with high speed npn and pnp SiGe:C HBTs," *IEEE International Electron Device Meeting Technical Digest,* pp. 117-120, December 2003.

[45] Kuo W.-M. L., Lu Y., Floyd B., Haugerud B., Sutton A., Krithivasan R., Cressler J. D., Gaucher B., Marshall P., Reed R., Rieh J.-S., and Freeman G., "Total dose tolerance of monolithic millimeter-wave transceiver building blocks in 200 GHz SiGe technology," *IEEE Trans. on Nuclear Science,* vol. 51, pp. 3781-3787, 2004.

[46] Nellis K. and Zampardi P., "A comparison of linear handset power amplifiers in different bipolar technologies," *IEEE Journal of Solid-State Circuits,* vol. 39, pp. 1746-1754, October 2004.

[47] Zerounian N., Aniel F., Barbalat B., Chevalier P., and Chantre A., "500 GHz cutoff frequency SiGe HBTs," *Electronics Letters,* vol. 43, pp. 774–775, July 2007.

[48] Hughes B., "A temperature noise model for extrinsic FET's," *IEEE Trans. on Microwave Theory and Techniques,* vol. 40, pp. 1821-1832, September 1992.

[49] Larson L., "Integrated Circuit Technology Options for RFIC's - Present Status and Future Directions," *IEEE Journal of Solid-State Circuits,* vol. 33, pp. 387-399, March 1998.

[50] Mattisson S., "Architecture and technology for multistandard transceivers," *Proceedings of the Bipolar/BiCMOS Circuits and Technology Meeting (BCTM),* pp. 82-85, September 2001.

[51] Lie D. Y. C., Yota J., Xia W., Joshi A. B., Williams R. A., Zwingman R., Chung L., and Kwong D. L., "New experimental findings on process-induced hot-carrier degradation of deep-submicron N-MOSFETs," *IEEE International Reliability Physics Symposium,* pp. 362-369, March 1999.

[52] Lie D. Y. C., Yuan X., Larson L. E., Wang Y. H., Senior A., and Mecke J., ""RF-SoC": low-power single-chip radio design using Si/SiGe BiCMOS technology," *Proceedings of the 3rd International Microwave and MillimeterWave Technology,* pp. 30-37, August 2002.

[53] Yuan X., Lie D. Y. C., Larson L. E., Blonski J., Gross J., Kumar M., Mecke J., Senior A., Chen Y., Pho A., and Harame D., "RF linearity study of SiGe HBTs for low power RFIC design I," *Proceedings of the 3rd International Microwave and Millimeter Wave Technology,* pp. 70-73, August 2002.

[54] Xu Z., Niu G., Luo L., Chakraborty P. S., Cheng P., Thomas D., and Cressler J. D., "Cryogenic RF Small-Signal Modeling and Parameter Extraction of SiGe HBTs," *IEEE Topical Meeting on Silicon Monolithic Integrated Circuits in RF Systems, SiRF'09,* pp. 1-4, Jan 2009.

[55] Kroemer H., "Two integral relations pertaining to electron transport through a bipolar transistor with a nonuniform energy gap in the base region," *Solid-State Electronics,* vol. 28, pp. 1101–1103, 1985.

[56] Mandal S. K., Marskole G. K., Chari K. S., and Maiti C. K., "Transit time components of a SiGe-HBT at low temperature," *Proc. 24th International Conference on Microelectronics,* vol. 1, pp. 315-318, May 2004.

[57] Webster W., "On the variation of junction-transistor current-amplification factor with emitter current," *Proc IRE,* vol. 42(6), pp. 914-920, 1954.

[58] Tang Z. R., Kamins T., and Salama C. A. T., "Analytical and experimental characteristics of SiGe HBT with thin α-Si : H emitters," *Solid-State Electronics,* vol. 38, pp. 1829-1834, 1995.

[59] Yuan J. S., "Effect of base profile on the base transit time of the bipolar transistor for all levels of injection," *IEEE Trans. on Electron Devices,* vol. 41, pp. 212-216, Feb 1994.

[60] Suzuki K., "Optimum base doping profile for minimum base transit time considering velocity saturation at base-collector junction and dependence of mobility and bandgap narrowing on doping concentration," *IEEE Trans. on Electron Devices,* vol. 48, pp. 2102-2107, 2001.

[61] Alamo J. D., Swirhum S., and Swanson R. M., "Simultaneous measurement of hole lifetime, hole mobility and bandgap narrowing in heavily doped n-type silicon," *IEDM Tech. Dig.,* pp. 290-293, 1985.

[62] Zareba A., Lukasiak L., and Jakubowski A., "Modeling of SiGe-base heterojunction bipolar transistor with gaussian doping distribution," *Solid-State Electronics,* vol. 45, pp. 2029-2032, 2001.

[63] Neamen D. A., *Semiconductor Physics and Devices: Basic Principles*, 3rd ed. New York: McGraw-Hill, 2003.

[64] Chen B. Y. and Kuo J. B., "An accurate knee current model considering quasi-saturation for BJTs operating at high current density," *Solid-State Electronics,* vol. 38, pp. 1282–1284, Jun 1995.

[65] Slotboom J. W. and Graaff H. C. D., "Measurement of bandgap narrowing in Si bipolar transistors," *Solid-State Electronics,* vol. 19, pp. 857–862, 1976.

[66] Lu T. C. and Kuo J. B., "A closed form analytical BJT forward transit time model considering bandgap narrowing effects and concentration dependent diffusion coefficients," *Solid-State Electronics,* vol. 35, pp. 1374–1377, 1992.

[67] Suzuki K., "Analytical base transit time model of uniformly-doped base bipolar transistors for high-injection regions," *Solid-State Electronics,* vol. 36, pp. 109-110, 1993.

[68] Muller R. and Kamins T., *Device electronics for intregrated circuits*, 2nd ed. New York: Wiley, 1986.

[69] Khan M. Z. R., "Base transit time of a bipolar junction transistor with nonuniformly doped base," in *M. Sc. Thesis, Department of EEE*: Bangladesh University of Engineering and Technology, Dhaka, Bangladesh, 2002.

[70] Nomani M. W. K., "A new technique for determining Base Transit Time of a BJT considering field dependent mobility," in *M. Sc. Thesis, Department of EEE*: Bangladesh University of Engineering and Technology, Dhaka, Bangladesh, 2006.

[71] Mohammedy F. M., "A distributed transmission line model for the base transit time of a nonuniformly doped bipolar junction transistor," in *M. Sc. Thesis, Department of EEE*: Bangladesh University of Engineering and Technology, Dhaka, Bangladesh, 2002.

[72] Kuo J. B. and Lu T. C., "A fully analytical partitioned-charge-based model for linearly-graded SiGe-base HBT," *Solid-State Electronics,* vol. 37, pp. 1561-1566, 1994.

[73] Ma P., "Analytical Model of Collector Current Density and Base Transit Time Based on Iteration Method," *Solid-State Electronics,* vol. 39, pp. 1683-86, 1996.

APPENDIX A

DERIVATION FOR LOW INJECTION

1. $-J_n = qD_n(x)\dfrac{n_{ie}^2(x)}{p(x)}\dfrac{d}{dx}\left[\dfrac{n(x)p(x)}{n_{ie}^2(x)}\right]$ ..(1.1)

Where, $p(x) = n(x) + N_B(x)$..(1.2)

2. $N_B(x) = N_B(0)\exp\left(-\dfrac{x^2}{2\sigma^2}\right)$..(2.1) where, $\sigma = \dfrac{W_B}{\sqrt{2\ln\dfrac{N_B(0)}{N_B(W_B)}}}$, and $m = \dfrac{1}{2\sigma^2}$

Therefore, $N_B(x) = N_B(0)\exp(-mx^2)$..(2.2)

3. $D_n(x) = D_{n0}\left(\dfrac{N_B(x)}{N_r}\right)^{-\gamma_1}$ ..(3.1) where, $\gamma_1 = 0.42$ and $D_{no} = 20.72\dfrac{cm^2}{\sec}$

$\Rightarrow D_n(x) = D_{n0}\left(\dfrac{N_B(0)\exp(-mx^2)}{N_r}\right)^{-\gamma_1}$ (using 2.2)

$\Rightarrow D_n(x) = D_{n0}\left(\dfrac{N_B(0)}{N_r}\right)^{-\gamma_1}\exp(m_1x^2)$

$\Rightarrow D_{nSi}(x) = D_n\exp(m_1x^2)$ ..(3.2) where, $D_n = D_{n0}\left(\dfrac{N_B(0)}{N_r}\right)^{-\gamma_1}$ and $m_1 = m\gamma_1$

4. $D_{nSiGe}(x) = bD_{nSi}(x)$..(4.1)

5. $v_{sa} = cv_s$..(5.1)

where,

$v_s = 10^7\dfrac{cm}{\sec}$

$c = \dfrac{0.342}{0.342 + y_{av}(1 - y_{av})}$

$y_{av} = \dfrac{y_c + y_e}{2}$

$b = 1 + 3y_{av}$

$y(x) = m_{Ge}x + y_E$

$y_D = y_{av}W_B$

$m_{Ge} = \dfrac{y_C - y_E}{W_B}$

6. $\mu_{nSi}(|E|,x)=\dfrac{v_s}{a|E(x)|+E_{cSi}(x)}$ ..(6.1) where, $a=0.7743$

7. $E_{cSi}(x)=\dfrac{v_s}{\mu_{nSi}(x)}$ ..(7.1)

Putting $E_{cSi}(x)$ in 6.1, we get

$$\mu_{nSi}(|E|,x)=\frac{v_s}{a|E(x)|+\dfrac{v_s}{\mu_{nSi}(x)}}$$

$$\Rightarrow D_{nSi}(|E|,x)=\frac{v_sV_T}{a|E(x)|+\dfrac{v_sV_T}{D_{nSi}(x)}}$$ where, $V_T=\dfrac{D_n(x)}{\mu_n(x)}$ (Einstein's Relation)

$$\Rightarrow D_{nSi}(|E|,x)=\frac{v_sV_T}{a|E(x)|+\dfrac{v_sV_T}{D_n}\exp(-m_1x^2)}$$ (using 3.2)

$$\Rightarrow D_{nSiGe}(|E|,x)=\frac{bv_{sa}V_T}{a|E(x)|+\dfrac{v_{sa}V_T}{D_n}\exp(-m_1x^2)}$$ ..(7.2) (using 4.1 and 5.1)

8. $\Rightarrow n_{ieSiGe}^2(x)=n_{ioSi}^2\gamma_r\exp\left(\dfrac{\Delta E_{geff}(x)}{kT}\right)$ ..(8.1) where,

$n_{ioSi}=1.4\times10^{10}cm^{-3}$

$\gamma_r=\exp(-\sqrt{5y_{av}})$

$\Delta E_{geff}(x)=\Delta E_{gHD}(x)+\Delta E_{gGe}(x)$

$\Delta E_{gGe}(x)=qV_{gGe}y(x)$

$V_{gGe}=688mV$

$\Delta E_{gHD}(x)=qV_{gHD}\ln\left(\dfrac{N_B(x)}{N_r}\right)$

$V_{gHD}=18mV$

Therefore, $\dfrac{\Delta E_{geff}(x)}{kT}=\dfrac{qV_{gHD}}{kT}\ln\left(\dfrac{N_B(0)\exp(-mx^2)}{N_r}\right)+\dfrac{qV_{gGe}y(x)}{kT}$

$$\Rightarrow \frac{\Delta E_{geff}(x)}{kT}=\ln\left(\frac{N_B(0)}{N_r}\exp(-mx^2)\right)^{\gamma_2}+\gamma_3y(x)$$ ..(8.2)

where, $\gamma_2=\dfrac{V_{gHD}}{V_t}$ and $\gamma_3=\dfrac{V_{gGe}}{V_t}$

Putting this into 8.1, we get,

$$\Rightarrow n_{ieSiGe}^2(x)=n_{ioSi}^2\gamma_r\left(\frac{N_B(0)}{N_r}\right)^{\gamma_2}\exp(-x^2m\gamma_2)\exp^{\gamma_3y(x)}$$

$$\Rightarrow n_{ieSiGe}^2(x) = n_{ioSi}^2 \gamma_r \left(\frac{N_B(0)}{N_r}\right)^{\gamma_2} \exp\left(-x^2 m \gamma_2\right) \exp^{\gamma_3 (m_{Ge} x + y_E)}$$

$$\Rightarrow n_{ieSiGe}^2(x) = n_{ioSi}^2 \gamma_r \exp(\gamma_3 y_E) \left(\frac{N_B(0)}{N_r}\right)^{\gamma_2} \exp\left(m_3 x - m_2 x^2\right)$$

where, $m_2 = m\gamma_2$ and $m_3 = m_{Ge}\gamma_3$

$$\Rightarrow n_{ieSiGe}^2(x) = n_{ieSiGe}^2(0) \exp\left(m_3 x - m_2 x^2\right) \quad ..(8.3)$$

where, $n_{ieSiGe}^2(0) = n_{ioSi}^2 \gamma_r \exp(\gamma_3 y_E) \left(\frac{N_B(0)}{N_r}\right)^{\gamma_2}$

9. $$E(x) = V_T \left(\frac{1}{p(x)} \frac{d}{dx} p(x) - \frac{1}{n_{ie}^2(x)} \frac{d}{dx} n_{ie}^2(x) \right) \quad ..(9.1)$$

For Low Injection, $p(x) = n_l(x) + N_B(x) \approx N_B(x)$. Therefore,

$$E_{lSiGe}(x) = V_T \left(\frac{1}{N_B(x)} \frac{d}{dx} N_B(x) - \frac{1}{n_{ieSiGe}^2(x)} \frac{d}{dx} n_{ieSiGe}^2(x) \right) \quad ..(9.2)$$

Using 2.2 and 8.3 we get,

$$\Rightarrow E_{lSiGe}(x) = V_T \left(\frac{1}{N_B(x)} \frac{d}{dx} N_B(0) \exp\left(-mx^2\right) - \frac{1}{n_{ieSiGe}^2(x)} \frac{d}{dx} n_{ieSiGe}^2(0) \exp\left(m_3 x - m_2 x^2\right) \right)$$

$$\Rightarrow E_{lSiGe}(x) = V_T \left\{ -2xm - \left(m_3 - 2m_2 x\right) \right\}$$

$$\Rightarrow E_{lSiGe}(x) = -V_T \left(m_3 + m_4 x\right) \quad ..(9.2) \qquad \text{where, } m_4 = 2(m - m_2)$$

Putting this in 7.2, we get,

$$\Rightarrow D_{nSiGe}(|E|, x) = \frac{b v_{sa} V_T}{a V_T (m_3 + m_4 x) + \frac{v_{sa} V_T}{D_n} \exp\left(-m_1 x^2\right)} \quad ..(7.3)$$

From 1.1, we have

10. $$-J_{nl} = q D_{nSiGe}(|E|, x) \frac{n_{ieSiGe}^2(x)}{N_B(x)} \frac{d}{dx} \left[\frac{n_l(x) N_B(x)}{n_{ieSiGe}^2(x)} \right] \quad ..(10.1)$$

$$\Rightarrow -J_{nl} = q D_{nSiGe}(|E|, x) \frac{n_{ieSiGe}^2(x)}{N_B(x)} n_{ieSiGe}^2(x) \left[\frac{n_{ieSiGe}^2(x) \left(n_l(x) \frac{d}{dx} N_B(x) + N_B(x) \frac{d}{dx} n_l(x) \right) - n_l(x) N_B(x) \frac{d}{dx} n_{ieSiGe}^2(x)}{\left(n_{ieSiGe}^2(x)\right)^2} \right]$$

$$\Rightarrow -J_{nl} = q D_{nSiGe}(|E|, x) \left(\frac{n_l(x)}{N_B(x)} \frac{d}{dx} N_B(x) + \frac{d}{dx} n_l(x) - \frac{n_l(x)}{n_{ieSiGe}^2(x)} \frac{d}{dx} n_{ieSiGe}^2(x) \right) \quad ..(10.2)$$

Using 2.2 and 8.3 in the above equation, we get,

$$\Rightarrow -J_{nl} = qD_{nSiGe}(|E|,x)\left(-2mxn_l(x)+\frac{d}{dx}n_l(x)-(m_3-2m_2x)n_l(x)\right)$$

$$\Rightarrow \frac{-J_{nl}}{qD_{nSiGe}(|E|,x)} = \frac{d}{dx}n_l(x)+n_l(x)(2m_2x-2mx-m_3) \quad ..(10.3)$$

Using 7.3, we can right the left hand side of the above equation as,

$$\Rightarrow \frac{-J_{nl}}{qD_{nSiGe}(|E|,x)} = \frac{-J_{nl}aV_T(m_3+m_4x)}{qbv_{sa}V_T} - \frac{J_{nl}v_{sa}V_T}{qbD_nV_Tv_{sa}}\exp(-m_1x^2)$$

$$\Rightarrow \frac{-J_{nl}}{qD_{nSiGe}(|E|,x)} = \frac{-J_{nl}a}{qbv_{sa}}(m_3+m_4x) - \frac{J_{nl}}{qbD_n}\exp(-m_1x^2)$$

Now using this result in 10.3, we finally have,

$$\Rightarrow \frac{d}{dx}n_l(x)-n_l(x)(m_4x+m_3) = \frac{-J_{nl}a}{qbv_{sa}}(m_3+m_4x) - \frac{J_{nl}}{qbD_n}\exp(-m_1x^2)$$

$$\Rightarrow \frac{d}{dx}n_l(x)-n_l(x)(m_4x+m_3) = -A_1J_{nl} - A_2xJ_{nl} - A_3J_{nl}\exp(-m_1x^2) \quad ..(10.4)$$

Where, $A_1 = \frac{am_3}{bqv_{sa}}$, $A_2 = \frac{am_4}{bqv_{sa}}$ and $A_3 = \frac{1}{bqD_n}$

The solution of equation 10.4 is:

$$n_l(x)\exp\left(-m_4\frac{x^2}{2}-m_3x\right)-n_l(0) = -J_{nl}\int_0^x \exp\left(-m_4\frac{x^2}{2}-m_3x\right)\left(A_1+A_2x+A_3\exp(-m_1x^2)\right)dx$$

$$\Rightarrow n_l(x) = n_l(0)\exp\left(m_4\frac{x^2}{2}+m_3x\right)-\exp\left(m_4\frac{x^2}{2}+m_3x\right)J_{nl}\int_0^x \exp\left(-m_4\frac{x^2}{2}-m_3x\right)\left(A_1+A_2x+A_3\exp(-m_1x^2)\right)dx$$

Let,

$$B_1(x) = \int_0^x A_1\exp\left(-m_4\frac{x^2}{2}-m_3x\right)dx,\ B_2(x) = \int_0^x A_2x\exp\left(-m_4\frac{x^2}{2}-m_3x\right)dx \ \text{ and}$$

$$B_3(x) = \int_0^x A_3\exp\left(-\left(m_1+\frac{m_4}{2}\right)x^2-m_3x\right)dx$$

Now, using integration tables/ Mathematica, we have,

$$B_1(x) = A_1\left[\sqrt{\pi}\frac{p_1}{m_3}\exp(p_1^2)\left\{erf\left(p_1+\frac{x}{\sqrt{2/m_4}}\right)-erf(p_1)\right\}\right], \quad \text{where, } p_1 = \frac{m_3}{\sqrt{2m_4}}$$

$$B_2(x) = \frac{A_2}{m_4}\left[1-\exp\left(-m_3x-m_4\frac{x^2}{2}\right)-m_3\frac{B_1(x)}{A_1}\right]$$

$$B_3(x) = A_3\left[\sqrt{\pi}\frac{p_2}{m_3}\exp(p_2^2)\left\{erf\left(p_2+\frac{x}{\sqrt{2/(m_4+2m_1)}}\right)-erf(p_2)\right\}\right],$$

where, $p_2 = \frac{m_3}{\sqrt{2m_4 + 4m_1}}$

Now putting these values in equation for $n_l(x)$, we get,

$$\Rightarrow n_l(x) = \exp\left(m_4 \frac{x^2}{2} + m_3 x\right)\left(n_l(0) - J_{nl}\left(B_1(x) + B_2(x) + B_3(x)\right)\right) \text{..(10.5)}$$

For x=W_B, 10.5 reduces to (also using $J_{nl} = qv_{sa} n_l(W_B)$),

$$\Rightarrow n_l(W_B) = \exp\left(m_4 \frac{{W_B}^2}{2} + m_3 W_B\right)\left(n_l(0) - qv_{sa} n_l(W_B)\left(B_1(W_B) + B_2(W_B) + B_3(W_B)\right)\right)$$

$$\Rightarrow n_l(W_B) = \frac{n_l(0)\exp\left(m_4 \frac{{W_B}^2}{2} + m_3 W_B\right)}{1 + qv_{sa}\exp\left(m_4 \frac{{W_B}^2}{2} + m_3 W_B\right)\left(B_1(W_B) + B_2(W_B) + B_3(W_B)\right)} \text{..(10.6)}$$

Using 10.6, we can calculate J_{nl} and then with 10.5 $n_l(x)$ can be found as well.

11. $Q_{Bnl} = q \int_0^{W_B} n_l(x)\,dx$ ..(11.1)

12. $\tau_{Bl} = \frac{Q_{Bnl}}{J_{nl}}$ ..(12.1)

APPENDIX B

DERIVATION FOR MODERATE INJECTION

1. $n(0) = \frac{n_{ieSiGe}^2(0)}{N_B(0)} \exp\left(\frac{V_{be}}{V_T}\right) f_w$ ..(1.1)

2. $f_w = \frac{1}{0.5 + \sqrt{0.25 + \frac{n_{ieSiGe}^2(0)}{N_B^2(0)} \exp\left(\frac{V_{be}}{V_T}\right)}}$ ..(2.1)

3. $n_m(x) = f_w n_l(x)$..(3.1)

4. $J_{nm} = f_w J_{nl}$ ..(4.1)

5. $n(x) = n_m(x) + \delta n(x)$..(5.1)

6. $p(x) = n_m(x) + \delta n(x) + N_B(x) = p_m(x) + \delta n(x)$..(6.1)

Therefore, $p_m(x) = n_m(x) + N_B(x)$..(6.2)

7. $-J_n = qD_{nSiGe}(|E|, x)\frac{n_{ieSiGe}^2(x)}{p_m(x) + \delta n(x)} \frac{d}{dx}\left[\frac{(n_m(x) + \delta n(x))(p_m(x) + \delta n(x))}{n_{ieSiGe}^2(x)}\right]$..(7.1)

$\Rightarrow -J_n = qD_{nSiGe}(|E|, x)\frac{n_{ieSiGe}^2(x)}{p_m(x)} \frac{d}{dx}\left[\frac{(n_m(x) + \delta n(x))p_m(x)}{n_{ieSiGe}^2(x)}\right]$ using $p(x) \approx p_m(x)$

$\Rightarrow -J_n = qD_{nSiGe}(|E|, x)\frac{n_{ieSiGe}^2(x)}{p_m(x)} \frac{d}{dx}\left[\frac{n(x)p_m(x)}{n_{ieSiGe}^2(x)}\right]$..(7.2) (using 5.1)

8. Let, $V_q(x) = \frac{p_m(x)}{n_{ieSiGe}^2(x)}$..(8.1)

9. $E(x) = V_T\left(\frac{1}{p(x)}\frac{d}{dx}p(x) - \frac{1}{n_{ie}^2(x)}\frac{d}{dx}n_{ie}^2(x)\right)$..(9.1)

$\Rightarrow E_{SiGe}(x) = V_T\left(\frac{1}{p_m(x)}\frac{d}{dx}p_m(x) - \frac{1}{n_{ieSiGe}^2(x)}\frac{d}{dx}n_{ieSiGe}^2(x)\right)$ using $p(x) \approx p_m(x)$

$\Rightarrow E_{SiGe}(x) = V_T\left(\frac{1}{V_q(x)n_{ieSiGe}^2(x)}\frac{d}{dx}V_q(x)n_{ieSiGe}^2(x) - \frac{1}{n_{ieSiGe}^2(x)}\frac{d}{dx}n_{ieSiGe}^2(x)\right)$ (using 9.1)

$$\Rightarrow E_{SiGe}(x) = \frac{V_T}{V_q(x)} \frac{d}{dx} V_q(x) ..(9.2)$$

As the E field is negative throughout x, we have,

$$\Rightarrow |E_{SiGe}(x)| = -\frac{V_T}{V_q(x)} \frac{d}{dx} V_q(x)$$

$$\Rightarrow \frac{|E_{SiGe}(x)|}{V_T} = -\frac{1}{V_q(x)} \frac{d}{dx} V_q(x) ..(9.3)$$

Now, using 8.1 in 7.2, we have

$$-J_n = \frac{qD_{nSiGe}(|E|, x)}{V_q(x)} \frac{d}{dx} [n(x)V_q(x)]$$

$$\Rightarrow \frac{d}{dx} [n(x)V_q(x)] = -\frac{J_n V_q(x)}{qD_{nSiGe}(|E|, x)} ..(7.3)$$

10. $D_{nSiGe}(|E|, x) = \dfrac{bv_{sa}V_T}{a|E_{SiGe}(x)| + \dfrac{v_{sa}V_T}{D_n} \exp(-m_1 x^2)}$ ..(10.1)

$$\Rightarrow \frac{1}{D_{nSiGe}(|E|, x)} = \frac{a|E_{SiGe}(x)|}{bv_{sa}V_T} + \frac{\exp(-m_1 x^2)}{bD_n} ..(10.2)$$

Now, using 10.2 in 7.3, we get

$$\frac{d}{dx} [n(x)V_q(x)] = -\frac{J_n}{q} \left(\frac{aV_q(x)|E_{SiGe}(x)|}{bv_{sa}V_T} + \frac{V_q(x)\exp(-m_1 x^2)}{bD_n} \right)$$

$$\Rightarrow \frac{d}{dx} [n(x)V_q(x)] = -\frac{J_n}{q} \left(-\frac{a}{bv_{sa}} \frac{d}{dx} V_q(x) + \frac{V_q(x)\exp(-m_1 x^2)}{bD_n} \right) \text{ (using 9.2)}$$

$$\Rightarrow n(x)V_q(x) = -\frac{J_n}{q} \left(-\frac{a}{bv_{sa}} V_q(x) - \frac{a}{bv_{sa}} C_1 + \frac{1}{bD_n} \int V_q(x)\exp(-m_1 x^2) dx \right) ..(10.3)$$

Where C_1 is an integrating constant.

11. $n^2_{ieSiGe}(x) = n^2_{ieSiGe}(0)\exp(m_3 x - m_2 x^2)$..(11.1)

Using 11.1 in 8.1, we get,

$$V_q(x) = \frac{p_m(x)}{n^2_{ieSiGe}(0)} \exp(m_2 x^2 - m_3 x)$$

$$\Rightarrow V_q(x) = \frac{1}{n^2_{ieSiGe}(0)} (n_m(x) + N_B(x))\exp(m_2 x^2 - m_3 x) \text{ (using 6.2)}$$

using 3.1 and $N_B(x)=N_B(0)\exp(-mx^2)$ we get,

$$\Rightarrow V_q(x)=\frac{1}{n_{ieSiGe}^2(0)}\left\{f_w n_l(x)+N_B(0)\exp(-mx^2)\right\}\exp(m_2x^2-m_3x) \quad ..(11.2)$$

Now putting results for $n_l(x)$ from low injection in 11.2, we get

$$\Rightarrow V_q(x)=\frac{1}{n_{ieSiGe}^2(0)}\left[f_w\left\{\exp\left(m_4\frac{x^2}{2}+m_3x\right)(n_l(0)-J_{nl}B(x))\right\}+N_B(0)\exp(-mx^2)\right]\exp(m_2x^2-m_3x)$$

where, $B(x)=B_1(x)+B_2(x)+B_3(x)$

$$\Rightarrow V_q(x)=\frac{1}{n_{ieSiGe}^2(0)}\left[f_w n_l(0)\exp\left(m_4\frac{x^2}{2}+m_3x\right)-J_{nl}f_wB(x)\exp\left(m_4\frac{x^2}{2}+m_3x\right)+N_B(0)\exp(-mx^2)\right]\exp(m_2x^2-m_3x)$$

Using 3.1 and 4.1 in the above equation, we have,

$$\Rightarrow V_q(x)=\frac{1}{n_{ieSiGe}^2(0)}\left[n_m(0)\exp\left(m_4\frac{x^2}{2}+m_2x^2\right)-J_{nm}B(x)\exp\left(m_4\frac{x^2}{2}+m_2x^2\right)+N_B(0)\exp(-mx^2+m_2x^2-m_3x)\right]$$

Using $\frac{m_4}{2}=m-m_2$ in the above equation, we get,

$$\Rightarrow V_q(x)=\frac{1}{n_{ieSiGe}^2(0)}\left[n_m(0)\exp(mx^2)-J_{nm}B(x)\exp(mx^2)+N_B(0)\exp\left(-\frac{m_4}{2}x^2-m_3x\right)\right] \quad ..(11.3)$$

Now multiplying both sides of 11.3 with $\exp(-m_1x^2)$ and integrating, we get,

$$\Rightarrow \int V_q(x)\exp(-m_1x^2)dx=$$

$$\frac{1}{n_{ieSiGe}^2(0)}\left[n_m(0)\int\exp\{(m-m_1)x^2\}dx-J_{nm}\int B(x)\exp\{(m-m_1)x^2\}dx+N_B(0)\int\exp\left(-\frac{m_4}{2}x^2-m_3x-m_1x^2\right)dx\right]$$

Let, $m_5=m-m_1$ and $m_6=\frac{m_4}{2}+m_1$

$$\Rightarrow \int V_q(x)\exp(-m_1x^2)dx=$$

$$\frac{1}{n_{ieSiGe}^2(0)}\left[n_m(0)\int\exp(m_5x^2)dx-J_{nm}\int B(x)\exp(m_5x^2)dx+N_B(0)\int\exp(-m_3x-m_6x^2)dx\right] \quad ..(11.4)$$

Putting 11.3 and 11.4 into 10.3, we get,

$$\Rightarrow n(x)V_q(x)=$$

$$-\frac{J_n}{q}\left(\begin{array}{l}-\frac{a}{bv_{sa}}\frac{1}{n_{ieSiGe}^2(0)}\left[n_m(0)\exp(mx^2)-J_{nm}B(x)\exp(mx^2)+N_B(0)\exp\left(-\frac{m_4}{2}x^2-m_3x\right)\right]-\frac{a}{bv_{sa}}C_1+\\ \frac{1}{bD_n}\frac{1}{n_{ieSiGe}^2(0)}\left[n_m(0)\int\exp(m_5x^2)dx-J_{nm}\int B(x)\exp(m_5x^2)dx+N_B(0)\int\exp(-m_3x-m_6x^2)dx\right]\end{array}\right)$$

$$\Rightarrow n(x)p_m(x)\exp\left(m_2x^2 - m_3x\right) =$$

$$-\frac{J_n}{qv_{sa}}\left(\begin{array}{l} -\frac{a}{b}\left[n_m(0)\exp\left(mx^2\right) - J_{nm}B(x)\exp\left(mx^2\right) + N_B(0)\exp\left(-\frac{m_4}{2}x^2 - m_3x\right)\right] + C_2 + \\ \frac{v_{sa}}{bD_n}\left[n_m(0)\int \exp\left(m_5x^2\right)dx - J_{nm}\int B(x)\exp\left(m_5x^2\right)dx + N_B(0)\int \exp\left(-m_3x - m_6x^2\right)dx\right] \end{array}\right)$$

Where, $C_2 = -\frac{a}{b}C_1 n_{ieSiGe}^2(0)$ is another constant.

Let, $\int \exp\left(m_5x^2\right)dx = E_1(x) + D_1$,

$\int B(x)\exp\left(m_5x^2\right)dx = E_2(x) + D_2$ and $\int \exp\left(-m_3x - m_6x^2\right)dx = E_3(x) + D_3$

Where, D's are all integration constants.

Putting all these values in the above equation, we have,

$$\Rightarrow n(x)p_m(x)\exp\left(m_2x^2 - m_3x\right) =$$

$$-\frac{J_n}{qv_{sa}}\left(\begin{array}{l} -\frac{a}{b}\left[n_m(0)\exp\left(mx^2\right) - J_{nm}B(x)\exp\left(mx^2\right) + N_B(0)\exp\left(-\frac{m_4}{2}x^2 - m_3x\right)\right] + C_2 + \\ \frac{v_{sa}}{bD_n}\left[n_m(0)E_1(x) - J_{nm}E_2(x) + N_B(0)E_3(x)\right] + D_4 \end{array}\right)$$

..(10.4)

Where, $D_4 = \frac{v_{sa}}{bD_n}n_m(0)D_1 - \frac{v_{sa}}{bD_n}J_{nm}D_2 + \frac{v_{sa}}{bD_n}N_B(0)D_3$ is another constant.

Putting x=0 in 10.4, we get,

$$\Rightarrow n(0)p_m(0) =$$

$$-\frac{J_n}{qv_{sa}}\left(-\frac{a}{b}\left[n_m(0) - J_{nm}B(0) + N_B(0)\right] + C_2 + \frac{v_{sa}}{bD_n}\left[n_m(0)E_1(0) - J_{nm}E_2(0) + N_B(0)E_3(0)\right] + D_4\right)$$

..(10.5)

Subtracting 10.5 from 10.4,

$$\Rightarrow n(x)p_m(x)\exp\left(m_2x^2 - m_3x\right) =$$

$$n(0)p_m(0) + \frac{J_n}{qv_{sa}}\left(\begin{array}{l} \frac{a}{b}\left[n_m(0)\left\{\exp\left(mx^2\right) - 1\right\} - J_{nm}\left\{B(x)\exp\left(mx^2\right) - B(0)\right\} + N_B(0)\left\{\exp\left(-\frac{m_4}{2}x^2 - m_3x\right) - 1\right\}\right] \\ -\frac{v_{sa}}{bD_n}\left[n_m(0)\left\{E_1(x) - E_1(0)\right\} - J_{nm}\left\{E_2(x) - E_2(0)\right\} + N_B(0)\left\{E_3(x) - E_3(0)\right\}\right] \end{array}\right)$$

..(10.6)

Therefore,

$$\Rightarrow n(x) = \frac{\exp\left(m_3x - m_2x^2\right)}{p_m(x)}\left(n(0)p_m(0) + \frac{J_n}{qv_{sa}}N(x)\right) \quad ..(10.7)$$

Where,

$$N(x)=\frac{a}{b}\left[n_m(0)\left\{\exp\left(mx^2\right)-1\right\}-J_{nm}\left\{B(x)\exp\left(mx^2\right)-B(0)\right\}+N_B(0)\left\{\exp\left(-\frac{m_4}{2}x^2-m_3x\right)-1\right\}\right]$$
$$-\frac{v_{sa}}{bD_n}\left[n_m(0)\left\{E_1(x)-E_1(0)\right\}-J_{nm}\left\{E_2(x)-E_2(0)\right\}+N_B(0)\left\{E_3(x)-E_3(0)\right\}\right]$$

..(10.8)

Let,

$$N_1(x)=n_m(0)\left\{\exp\left(mx^2\right)-1\right\}-J_{nm}\left\{B(x)\exp\left(mx^2\right)-B(0)\right\}+N_B(0)\left\{\exp\left(-\frac{m_4}{2}x^2-m_3x\right)-1\right\}$$

and

$$N_2(x)=n_m(0)\left\{E_1(x)-E_1(0)\right\}-J_{nm}\left\{E_2(x)-E_2(0)\right\}+N_B(0)\left\{E_3(x)-E_3(0)\right\}$$

So that, 10.7 reduces to,

$$N(x)=\frac{a}{b}N_1(x)-\frac{v_{sa}}{bD_n}N_2(x) \quad ..(10.9)$$

Putting x=W_B in 10.7 (also using $J_n=qv_{sa}n(W_B)$), we get,

$$\Rightarrow n(W_B)=\frac{\exp\left(m_3W_B-m_2W_B{}^2\right)}{p_m(W_B)}\left(n(0)p_m(0)+\frac{qv_{sa}n(W_B)}{qv_{sa}}N(W_B)\right)$$

$$\Rightarrow n(W_B)=\frac{n(0)p_m(0)\exp\left(m_3W_B-m_2W_B{}^2\right)}{p_m(W_B)-N(W_B)\exp\left(m_3W_B-m_2W_B{}^2\right)} \quad ..(10.10)$$

Using 10.10, we can calculate J_n and then with 10.7 n(x) can be found as well.

12. $$Q_{Bn}=q\int_0^{W_B}n(x)dx \quad ..(12.1)$$

13. $$\tau_B=\frac{Q_{Bn}}{J_n} \quad ..(13.1)$$